Temporal observations of bright soil exposures at Gusev crater, Mars

M. S. Rice,[1] J. F. Bell III,[1] E. A. Cloutis,[2] J. J. Wray,[1] K. E. Herkenhoff,[3] R. Sullivan,[1] J. R. Johnson,[3] and R. B. Anderson[1]

Received 24 June 2010; revised 10 September 2010; accepted 5 November 2010; published 27 January 2011.

[1] The Mars Exploration Rover Spirit has discovered bright soil deposits in its wheel tracks that previously have been confirmed to contain ferric sulfates and/or opaline silica. Repeated Pancam multispectral observations have been acquired at four of these deposits to monitor spectral and textural changes over time during exposure to Martian surface conditions. Previous studies suggested that temporal spectral changes occur because of mineralogic changes (e.g., phase transitions accompanying dehydration). In this study, we present a multispectral and temporal analysis of eight Pancam image sequences at the Tyrone exposure, three at the Gertrude Weise exposure, two at the Kit Carson exposure, and ten at the Ulysses exposure that have been acquired as of sol 2132 (1 January 2010). We compare observed variations in Pancam data to spectral changes predicted by laboratory experiments for the dehydration of ferric sulfates. We also present a spectral analysis of repeated Mars Reconnaissance Orbiter HiRISE observations spanning 32 sols and a textural analysis of Spirit Microscopic Imager observations of Ulysses spanning 102 sols. At all bright soil exposures, we observe no statistically significant spectral changes with time that are uniquely diagnostic of dehydration and/or mineralogic phase changes. However, at Kit Carson and Ulysses, we observe significant textural changes, including slumping within the wheel trench, movement of individual grains, disappearance of fines, and dispersal of soil clods. All observed textural changes are consistent with aeolian sorting and/or minor amounts of air fall dust deposition.

Citation: Rice, M. S., J. F. Bell III, E. A. Cloutis, J. J. Wray, K. E. Herkenhoff, R. Sullivan, J. R. Johnson, and R. B. Anderson (2011), Temporal observations of bright soil exposures at Gusev crater, Mars, *J. Geophys. Res.*, *116*, E00F14, doi:10.1029/2010JE003683.

1. Introduction and Background

[2] The Mars Exploration Rover (MER) Spirit has excavated subsurface deposits of sulfate- and/or silica-rich materials in eighteen locations in the Columbia Hills of Gusev crater, Mars. These deposits occur as anomalously high albedo soil exposures within the rover's wheel tracks, with white and/or yellow hues that vary over small length scales. Most of these deposits have been brought up from depths of ~10 cm by the dragging motion of Spirit's inoperative right front wheel, its actuator having failed on sol 779 of the mission. In situ measurements with Spirit's Alpha Particle X-ray Spectrometer (AXPS) have revealed that these soils have the highest sulfur concentrations (up to 38 wt.% SO_3) of any materials yet observed by either of the MER rovers [*Ming et al.*, 2006, 2008; *Arvidson et al.*, 2010]. Mössbauer (MB) spectrometer data suggest the presence of ferric-bearing sulfates [e.g., *Gellert et al.*, 2006; *Morris et al.*, 2006, 2008], and the soils' distinctive Panoramic Camera (Pancam) and Miniature Thermal Emission Spectrometer (Mini-TES) spectra are consistent with a heterogeneous mixture of hydrated ferric sulfates [e.g., *Johnson et al.*, 2007; *Lane et al.*, 2008; *Parente et al.*, 2009].

[3] At the soil exposure called Gertrude Weise, the highest albedo soil observed by Spirit, APXS measurements revealed a nearly pure silica composition (~98 wt.% SiO_2 when corrected for dust contamination) and minor TiO_2 [*Squyres et al.*, 2008]. Mini-TES measurements of this soil are consistent with the presence of hydrated amorphous silica [*Squyres et al.*, 2008; S. W. Ruff et al., Characteristics, distribution, and significance of opaline silica in Gusev crater, manuscript in preparation, 2010], and a ~1 μm absorption feature in Pancam spectra indicates the presence of H_2O and/or OH [*Rice et al.*, 2010a]. While Gertrude Weise is the only nearly pure silica soil yet discovered, the sulfate-bearing exposures at regions called Tyrone and Ulysses also contain a component enriched in SiO_2 [*Squyres et al.*, 2008; *Wang et al.*, 2008; *Arvidson et al.*, 2010; S. W. Ruff et al., manuscript in preparation, 2010].

[1]Department of Astronomy, Cornell University, Ithaca, New York, USA.
[2]Department of Geography, University of Winnipeg, Winnipeg, Manitoba, Canada.
[3]Astrogeology Science Center, U.S. Geological Survey, Flagstaff, Arizona, USA.

0148-0227/11/2010JE003683

Table 1. Pancam Filter Data

Filter	Effective Wavelength[a] (nm)	Band Pass[a] (nm)	Camera
L7	432	32	LEFT
R1	436	37	RIGHT
L6	482	30	LEFT
L5	535	20	LEFT
L4	601	17	LEFT
L3	673	16	LEFT
L2	753	20	LEFT
R2	754	20	RIGHT
R3	803	20	RIGHT
R4	864	17	RIGHT
R5	904	26	RIGHT
R6	934	25	RIGHT
R7	1009	38	RIGHT

[a]From *Bell et al.* [2003].

[4] The mineralogy, geochemistry, spatial variability, and geologic setting of the bright subsurface soils suggest that they likely formed in a hydrothermal environment from fumarolic condensates, precipitation from geothermal waters, and/or leaching of local basaltic rocks [e.g., *Squyres et al.*, 2008; *Yen et al.*, 2008; *Morris et al.*, 2008]. The time of hydrothermal activity within Gusev crater, when the sulfate- and silica-rich soils would have formed, is not well constrained; however, the processes that have sorted, transported and modified the bright soil material may be ongoing. Indeed, the layered structure of the Ulysses soil, where soluble ferric sulfate species appear to be segregated below a layer with a less soluble silica-rich component, all below an insoluble, cemented hematite and calcium sulfate surface layer, suggests an ongoing pedogenic modification from downward migration of soluble materials by gravity-driven water [*Arvidson et al.*, 2010].

[5] Some ferric sulfate species that have been proposed as possible components of the Spirit bright soil exposures, such as ferricopiapite [$Fe^{2+}_{2/3}Fe^{3+}_4(SO_4)_6(OH)_2 \cdot 20(H_2O)$] and fibroferrite [$Fe^{3+}(SO_4)(OH) \cdot 5H2O$] [*Johnson et al.*, 2007; *Lane et al.*, 2008; *Parente et al.*, 2009], are known to be unstable under current Martian surface conditions [*Chipera et al.*, 2007; *Cloutis et al.*, 2008; *Freeman et al.*, 2009; A. Wang et al., Ferric sulfates on Mars: Analysis of Pancam spectral data from the Spirit Rover supported by laboratory investigations, submitted to *Journal of Geophysical Research*, 2010]. If the relative humidity environment in the near subsurface differs from that of the surface (i.e., is buffered by hydrated minerals or ground ice), it is possible that buried soils are not in equilibrium with surface conditions at the Spirit site, and that some minerals could undergo dehydration and/or phase changes after exhumation by the rovers' wheels.

[6] Spectral changes are known to accompany mineralogic changes among ferric sulfates and hydrated silica phases, resulting in modifications to their visible color [*Cloutis et al.*, 2008; *Rice et al.*, 2010b; A. Wang et al., submitted manuscript, 2010]. *Wang et al.* [2008] suggested that such modifications occurred for the Tyrone soil, and they described changes in the blue-to-red (432 to 753 nm) spectral slope in Pancam observations spanning a period of ~150 sols. Textural changes, such as shrinkage and cracking, are also expected to accompany the dehydration of hydrated ferric sulfates based on laboratory experiments [e.g., *Cloutis et al.*, 2008].

[7] To test the hypothesis that the Spirit bright soils have undergone mineralogic changes upon exposure to the Martian surface, we have performed a detailed analysis of Pancam multispectral images at the four sites where repeat observations have been made: Tyrone (sols 790–1062), Gertrude Weise (sols 1158–1198), Kit Carson (sols 1864–1866), and Ulysses (sols 1888–2132). We include a multispectral analysis of repeated Mars Reconnaissance Orbiter (MRO) High Resolution Imaging Science Experiment (HiRISE) observations of these soils for sols 1935 to 1967 and compare the analyses to Pancam observations. We also compare temporal observations in both the Pancam and HiRISE multispectral data to the variations predicted from laboratory experiments on ferric sulfate minerals exposed to current Martian surface conditions.

[8] For the Pancam images with high enough spatial resolution to resolve soil texture (at Kit Carson and Ulysses), we describe textural changes observed with time and discuss whether they are indicative of mineralogic changes, aeolian sorting, and/or dust deposition within the soil trenches. Although detailed studies of the wind-driven mobility of basaltic sand and air fall dust have been performed at Gusev crater [e.g., *Greeley et al.*, 2006; *Sullivan et al.*, 2008], no assessment has yet been made of the mobility of the bright soils, which we address here. We also use the available repeated observations of these soils from Spirit's Microscopic Imager (MI) to observe and document additional textural changes, allowing us to characterize temporal changes in the bright soils from the microscopic to orbital scale.

2. Methods

2.1. Pancam Observations

2.1.1. Pancam Instrument and Calibration

[9] The Pancam instrument consists of two cameras at a 30 cm stereo separation, each using a 1024 × 1024 pixel charge-coupled device (CCD) detector with 0.27 mrad per pixel resolution [*Bell et al.*, 2003, 2006]. Pancam's 13 narrowband geology filters cover 11 specific wavelengths in the visible and near infrared (432 to 1009 nm; Table 1). Some of the images used in this study were acquired using lossy wavelet-based ("ICER") compression [*Maki et al.*, 2003]. Based on prelaunch tests, compression effects on radiometric precision at the typical compression bit rates employed using the ICER compressor were estimated to be less than 1% [*Bell et al.*, 2006].

[10] We use near-simultaneous observations of the Pancam calibration target, as well as prelaunch calibration and modeling, to derive estimated reflectances of the scene relative to the standard reflectance materials on the calibration target [*Bell et al.*, 2003, 2006]. To correct for dust contamination of the calibration target, Pancam data are calibrated using a two-layer radiative transfer model [*Sohl-Dickstein et al.*, 2005; *Bell et al.*, 2006; *Kinch et al.*, 2007]. The Pancam reflectance products are called "IOF" images, where IOF (also known as the "radiance factor" or "I over F") [*Hapke*, 1993], is defined as the ratio of the bidirectional reflectance of a surface to that of a normally illuminated, perfectly diffuse surface. Dividing the Pancam IOF images by the cosine of the solar incidence angle at the time of each observation gives the relative reflectance R^* [*Reid et al.*, 1999; *Bell et al.*, 2006], also known as the "reflectance factor" or "reflectance coef-

Table 2. Pancam Full Filter Imaging Sequences Used for Spectral Characterization of Bright Soils[a]

Sol	Site[b]	Position[b]	Sequence ID	Local True Solar Time[c]	Imaging Duration (s)	Incidence Angle[c] (deg)	Emission Angle[c,d] (deg)	Phase Angle[c] (deg)	Sols After Exposure	Tau[e]	Saturated Filters[f]
					Tyrone						
790	126	142	P2531	11:56:05	236	26.9	28.2	41.5	8	0.342	L67
864	128	0	P2547	12:37:47	231	38.3	5.8	64.0	82	0.256	L6
922	128	0	P2552	12:02:10	288	39.9	5.4	71.6	140	0.295	L6
959	128	0	P2560	12:07:35	249	38.9	5.4	70.7	177	0.302	—
982	128	0	P2566	12:10:36	211	37.0	5.4	70.5	200	0.312	—
1005	128	0	P2576	12:23:12	353	34.7	5.4	68.3	223	0.240	—
1036	128	20	P2585	13:03:39	200	33.1	6.1	60.2	254	0.381	—
1062	128	115	P2596	12:30:12	412	25.1	5.6	70.5	280	0.883	—
					Gertrude Weise						
1158	128	1318	P2581	12:29:46	274	7.3	12.0	74.9	10	0.800	—
1187	129	112	P2533	12:16:34	261	6.4	19.6	64.6	39	0.939	—
1198	129	140	P2539	12:11:16	394	7.4	42.2	55.1	50	0.943	—
					Kit Carson						
1864	136	614	P2562[g]	12:32:30	183	10.1	48.0	31.9	3	1.187	—
1866	136	614	P2555	12:43:18	286	12.3	57.3	20.7	5	1.103	—
					Ulysses						
1888	137	130	P2559	14:01:10	878	30.0	65.6	42.1	2	0.875	—
1892	137	178	P2560	13:07:52	254	18.7	54.6	34.3	6	0.823	—
1894	137	182	P2560	13:04:35	252	18.1	54.6	34.1	8	0.792	—
1897	137	195	P2562	12:24:41	262	11.6	58.3	24.6	11	0.768	—
1933	137	249	P2382[h]	13:32:11	4372	23.8	58.5	40.4	47	0.470	—
1982	137	249	P2547	13:15:13	254	18.3	66.3	26.3	96	0.377	R1
2019	137	249	P2392[h]	11:41:49	4360	6.1	58.7	32.8	142	1.452	L567R1[i]

[a]Feature names are informal and not formally accepted by the International Astronomical Union.
[b]The surface coordinate frames utilized by MER [*Maki et al.*, 2003].
[c]At the starting time of the Pancam observation and for the center of the image.
[d]The INSTRUMENT_ELEVATION parameter stored in the image label.
[e]Visible optical depth observed with Pancam's L8 filter [*Lemmon et al.*, 2004].
[f]Where clusters of pixels in the raw image equal 4095 DN.
[g]This sequence includes a reduced filter set: L257R12467.
[h]These sequences contain five pointings to cover the extent of the soil exposure.
[i]The saturated pixels in this sequence were over reflective portions of the spacecraft, not the soil exposures.

ficient" [*Hapke*, 1993]. *Bell et al.* [2006] have estimated the relative filter-to-filter uncertainties in R^* to be 1–5%, and the absolute reflectance levels to be accurate to within ~10%. Because diffuse component corrections are relatively minor at the solar incidence angles of our data set (6°–40°; Table 2) [*Johnson et al.*, 2006], we did not correct for diffuse illumination.

2.1.2. Extraction of Pancam Spectra

[11] We have acquired visible to near-infrared (Vis-NIR) spectra of the soil targets by manually selecting pixels from common regions of interest (ROIs) in the right and left camera data sets and averaging the R^* values of those regions for each filter. We have chosen ROIs for each target that include as many pixels as possible (to minimize instrumental artifacts and statistical noise), excluding shadowed regions. We also exclude pixels that are potentially approaching saturation to ensure that we only use data within the demonstrated linearity of the Pancam instrument [*Bell et al.*, 2003]. For the Tyrone, Kit Carson, and Ulysses soils, we have selected ROIs from both the "yellow" and "white" hue separations (indicated by the yellow and black outlines, respectively, in Figures 2, 6, 9 and 12). In all images, we also extracted representative spectra from other scene elements (undisturbed dusty soil and disturbed dark soil, indicated by the red and brown outlines). For the blue (432 and 436 nm) and red (753 and 754 nm) stereo filters, we have used the R^* values acquired by the left camera (432 and 753 nm). The error bars represent the variance among the selected ROI pixels, rather than from the formal instrumental noise (which is generally much lower) [*Bell et al.*, 2006].

2.1.3. Comparisons of Spectral Parameters

[12] To quantify spectral variations with time, we have chosen four spectral parameters to compare between image sequences (Table 3). Three of these parameters characterize distinctive regions of the Vis-NIR spectra of ferric sulfates: (1) the 753 to 432 nm ratio, which quantifies the overall "redness" of the sample's color; (2) the 535 nm band depth, which indicates the strength of Fe^{3+} absorptions near ~550 nm; and (3) the 864 nm band depth, which quantifies the diagnostic Fe^{3+}-related absorptions at ~850–900 nm. Strong 535 nm and 864 nm band depths have been used in previous studies to classify the Pancam spectra of sulfate-rich soils at Gusev crater [*Farrand et al.*, 2008; *Parente et al.*, 2009]. We have also acquired laboratory spectra of four candidate ferric sulfates during long-term exposure to Martian surface conditions in order to characterize the temporal behavior of these spectral parameters for specific minerals (described in section 2.4).

[13] The fourth spectral parameter that we monitor is the 934 to 1009 nm ratio. This parameter has previously been used to detect silica-rich materials along the rover's traverse in Gusev crater [*Wang et al.*, 2008; *Rice et al.*, 2010a]. A high 934 to 1009 nm ratio (or steeply negative 934 to 1009 nm slope) is attributed to a combinational mode of H_2O ($2\nu_1 + \nu_3$)

Table 3. Spectral Parameters Used in This Study

Parameter	Description
535 nm band depth	$1 - (R^*_{535}/[(0.573 \times R^*_{432}) + (0.427 \times R^*_{673})])$
753 nm to 432 nm ratio	$(R^*_{753})/(R^*_{432})$
864 nm band depth	$1 - (R^*_{864}/[(0.387 \times R^*_{753}) + (0.613 \times R^*_{934})])$
934 to 1009 nm ratio	$(R^*_{934})/(R^*_{1009})$

and/or an OH overtone (3ν) near ~970–1000 nm, and its magnitude is sensitive to the amount of OH/H_2O present in the mineral and/or adsorbed on mineral grains [*Rice et al.*, 2010a]. For a detailed explanation of the attribution of a negative 934 to 1009 nm slope to water and/or OH, as opposed to other factors that can affect the spectral slope (such as viewing geometry, dust coatings or an uncorrected diffuse component), we refer the reader to *Rice et al.* [2010a]. Because the depths of all H_2O and OH absorption features in silica decrease during dehydration experiments [e.g., *Cloutis et al.*, 2008; *Rice et al.*, 2010b], an observed decrease in the magnitude of the 934 to 1009 nm ratio with time would be consistent with the soils dehydrating upon exposure.

[14] We estimate the uncertainty in the spectral parameters by propagating the uncertainty in R^* through the calculations shown in Table 3 by standard error analysis (e.g., the fractional uncertainty in the 753 to 432 nm ratio is calculated as the sum in quadrature of the fractional uncertainties in R^*_{753} and R^*_{432}).

2.1.4. Correction for Minor Dust Contamination of Camera Optics

[15] All images used in this study exhibit some effects attributed to minor heterogeneous dust contamination on the front sapphire windows of the Pancam instruments. The effect is too small to be meaningful in individual filter images, but it is enhanced in the ratio and band depth maps used in this study, where top-to-bottom brightness gradients of up to 5–10% have been observed in some scenes. This gradient does not affect our spectral comparisons when the ROIs are selected from the same region of the CCD in each image (as is the case for the Tyrone and Ulysses observations), but it must be accounted for when we compare spectra from different locations in each image.

[16] In this study we account for dust contamination effects on the optics by considering the spectral parameters as ratios of the bright soil targets to dusty, undisturbed soils imaged in similar regions of the field of view (FOV), rather than as absolute values. We assume that the spectra of undisturbed, dust-covered surface soils should not change between image sequences under the same or nearly the same lighting conditions. Because undisturbed soils are primarily of basaltic composition [e.g., *Sullivan et al.*, 2008; *Morris and Klingelhöfer*, 2008] and have likely been exposed to surface conditions for an extensive time, we assume that they are in equilibrium and do not undergo mineralogic changes during our short observation periods. Thus we can enhance our ability to detect changes in the sulfate- and silica-rich soils by observing them relative to unchanging, undisturbed materials. The uncertainty in these ratios is estimated by propagating the uncertainties in the values of the spectral parameters for the bright and undisturbed soils, which is a conservative but prudent overestimate of the true instrumental error.

2.1.5. Coregistration of Multiple Image Sequences

[17] To monitor pixel-to-pixel changes between Pancam image sequences, we have coregistered the image sequences from Tyrone that were acquired from nearly identical positions. During Spirit's second winter campaign, the rover was parked at Low Ridge in view of the Tyrone soil exposure at Low Ridge (Figure 1) and made five Pancam 13-filter observations from sols 864–1005 (Table 2). We have shifted each of those image sequences by an integer number of pixels in the x and y directions to coregister all images for direct spectral comparisons. In all cases the required shifts were small (<30 pixels, <3% of the FOV), and thus there were no significant variations in emission angle geometry among these observations. The effect of coregistration on radiometric precision is minor given that the shifts were integer-only and the images were not resampled. Tyrone was the only soil target from which multiple Pancam observations were acquired from similar enough perspectives to perform a coregistration.

[18] To illustrate trends in temporal variations of the spectral parameters listed in Table 3, we have calculated the percent change of each parameter for each pixel in the coregistered Tyrone image set. For every pixel, we have performed a linear regression fit to the spectral parameter versus sol data, and we calculate the percent difference between the values of the linear function at the first and last sols of observation. We use the resulting "percent change maps" in addition to spectra from selected ROIs (section 2.1.2) to look for systematic spectral variations relative to the rest of the scene in the Tyrone observations.

2.2. HiRISE Observations

2.2.1. HiRISE Instrument and Calibration

[19] Orbital monitoring provides an independent view of the spectral evolution of bright soils exposed by Spirit, and enables monitoring to continue even after the rover has

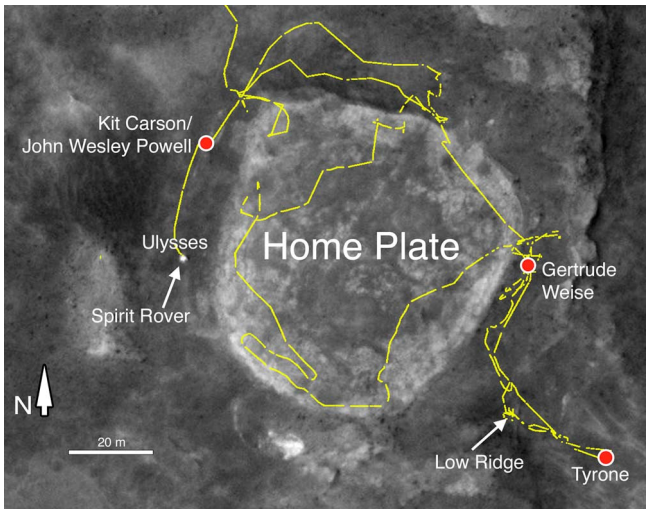

Figure 1. Spirit traverse map of the Home Plate vicinity (sols 743–2185) showing locations of the soil exposures discussed in this work and the Spirit rover embedded in the Ulysses soil as of sol 2185. Traverse is shown over a subframe of HiRISE image ESP_0013499_1650_red.

Table 4. HiRISE Observations of Kit Carson Soils

Image ID	Sol	Local True Solar Time	RED Pixel Scale (cm)	IR/BG Pixel Scale (cm)	Incidence Angle (deg)	Emission Angle (deg)	Phase Angle (deg)	Atmospheric Opacity (τ)
ESP_013499_1650	1935	14:39	26.9	53.8	38.7	10.1	48.5	0.51
ESP_013921_1650	1967	14:28	26.5	26.5	35.8	8.5	27.4	0.39

driven out of Pancam imaging range. Specifically, the MRO HiRISE camera [*McEwen et al.*, 2007] has a sufficiently small pixel scale (~26.5 cm at the latitude of the Columbia Hills) to enable detection of the largest exposures of bright soils. HiRISE has three color filters: blue-green (BG; λ_{eff} = 502 ± 157 nm), red (RED; λ_{eff} = 686 ± 267 nm), and near-infrared (IR; λ_{eff} = 878 ± 143 nm) [*McEwen et al.*, 2007; *Delamere et al.*, 2010], allowing detection of color changes over a limited portion of the spectrum. BG and IR data can only be acquired for a central strip covering 20% of each HiRISE RED image. In this study we compare the two observations with color coverage of the Home Plate vicinity during the period over which the Kit Carson soils were visible from orbit (Table 4).

[20] The current state of radiometric calibration for HiRISE was recently described by *Delamere et al.* [2010]. Uncertainties in absolute I/F values were estimated as ±20% absolute, whereas relative errors within a HiRISE image are typically only ~2% (~0.5% within a single CCD channel). This high relative precision can be exploited for change detection studies by observing not just the change in absolute I/F of a feature of interest, but also the change in I/F ratio between a feature of interest and an undisturbed homogeneous area of adjacent terrain within the same CCD channel. This technique has been used successfully to monitor color and albedo changes of 20–60% attributed to sublimation of subsurface water ice exposed by impact cratering [*Byrne et al.*, 2009].

[21] To correct for the spectral contribution from atmospheric aerosols, which can either brighten or darken the apparent I/F of a given pixel depending on the surface albedo, we use the method described by *Portyankina et al.* [2010], which has previously been tested on the set of images used in this study and demonstrably reduces I/F discrepancies between them. We have performed our analysis with and without the *Portyankina et al.* dust correction, and find that the correction changes relative I/F values in the RED and IR filters by <1% and in the BG filter by 3–5% for both observations. The estimated added uncertainty in I/F due to the dust correction is ~1%.

2.2.2. Comparison of HiRISE Color Data

[22] We resampled each HiRISE image (Table 4) to 50 cm/pixel so that they could be compared directly. This pixel size is large compared to the bright soil exposures, suggesting that most or all "bright soil" pixels are actually spatial mixtures of bright soil plus adjacent undisturbed soils and/or rocks (which are universally darker). We therefore measured I/F only for the brightest pixel within each soil exposure in a given image in order to minimize spectral contamination from other materials. There was no saturation in any HiRISE band for the soils observations. To reduce the effects of differing illumination and observation geometry between images (Table 4), we divided these bright soil I/F values by those extracted from nearby areas of the surface that appear relatively uniform and were not disturbed by Spirit. We tested several of these denominators (each an average of ~100 pixels) to confirm that our results do not depend on the choice of denominator.

[23] We measured the BG, RED and IR relative I/F for the Kit Carson, Gertrude Weise and Tyrone soils, which had been exposed to the surface for 74, 787 and 1153 sols, respectively, when the first HiRISE observation was made. For additional points of comparison, we extracted single-pixel I/F values for four nearby bright "calibration" outcrops undisturbed by Spirit, which would not be expected to undergo intrinsic spectral changes. We also measured the ratios of relative RED to relative BG for comparison with Pancam red to blue ratios (753 nm to 432 nm), as well as relative IR to relative RED.

2.3. Microscopic Imager Observations

[24] The Microscopic Imager (MI) is a fixed focus camera mounted on the instrument arm, with the same 1024 x 1024 CCD as the other MER cameras [*Herkenhoff et al.*, 2003]. The MI acquires panchromatic images at a scale of 31 microns/pixel over a broad spectral range (400 to 700 nm). The MI acquires images using solar or diffuse skylight illumination of the target surface. The MI focal section merges used in this study combine the best focused parts of images acquired at multiple distances from the target, separated by the 3 mm depth of field of the MI. Some MI images were merged with Pancam color data using the approach described by *Herkenhoff et al.* [2006]. Details of all MI observations used in this study are provided in Table 5.

2.4. Laboratory Exposure of Ferric Sulfates to Martian Surface Conditions

[25] To better characterize the expected spectral behavior of ferric sulfate materials as they dehydrate upon exposure to current Martian surface conditions, and to predict the spectral changes observable to the Pancam and HiRISE instruments, we have subjected four ferric sulfate samples to long-duration (150+ days) simulated Martian pressure and temperature conditions: (1) coquimbite [$Fe_2^{3+}(SO_4)_3 \cdot 9H_2O$]; (2) ferricopiapite [$Fe_{2/3}^{3+}Fe_4^{3+}(SO_4)_6(OH)_2 \cdot 20(H_2O)$]; (3) fibroferrite [$Fe^{3+}(SO_4)(OH) \cdot 5H2O$]; and (4) rhomboclase [$HFe^{3+}(SO_4)_2 \cdot 4H_2O$]. These specific ferric sulfates were chosen based on their identification as possible mineral constituents of the Gusev bright soil deposits from Pancam spectral deconvolution studies [*Johnson et al.*, 2007; *Lane et al.*, 2008; *Parente et al.*, 2009]. All samples were characterized by X-ray fluorescence and X-ray diffraction, and water contents were measured as the weight losses upon heating the samples to 900°C for 1 to 1.5 h, as described by *Mertzman* [2000]. The compositions and phases of each sample are provided in Table 6.

[26] The samples were ground and sieved to <45 μm and exposed to simulated Mars surface conditions using the

Table 5. Microscopic Imager Observations

Soil Exposure Name	Target Name	Sol	Starting Image ID	Relation to MB	Sols After Exposure
Kit Carson/John Wesley Powell	John Wesley Powell	1863	2M291757231	post MB	3
Ulysses	Sackrider	1922	2M296987659	post MB	36
		1925	2M297265696	post MB	39
		1982	2M302317675	no MB	96
			2M302318000	no MB	96
			2M302318330	no MB	96
			2M302318917	no MB	96
	Penina	1936	2M298228753	post MB	50
		1940	2M298597018	post MB	54
		1941	2M298683977	post MB	55
		1986	2M302672548	no MB	100
			2M302672856	no MB	100
		2024	2M306051847	no MB	138

University of Winnipeg's Miniature Mars Environment (mini-ME) chamber [*Craig et al.*, 2001]. A constant atmospheric pressure was maintained at 660 Pa CO_2 (6.6 mbar; 5 Torr), and the sample temperature was restricted to close to maximum surface temperatures on present-day Mars (~20°C), as described by *Cloutis et al.* [2008]. We note that the partial pressure of water vapor (pH_2O) was not monitored during the experiment; however, a constant supply of dry CO_2 was supplied to the samples and Mars atmospheric pressure maintained with a vacuum pump, and thus the expected relative humidity is near zero.

[27] Reflectance spectra were measured with an Analytical Spectral Devices (ASD) FieldSpec Pro HR spectrometer (at a viewing geometry of i = 0° and e = 0° using a bifurcated probe) through a 10 mm thick sapphire window. Sample spectra were measured relative to a halon standard and corrected for minor (<2%) irregularities in its absolute reflectance. Spectra were collected every few days for the

Table 6. Composition of Samples Used in This Study

Component[a]	Coquimbite SPT126	Ferricopiapite SPT125	Fibroferrite SPT121	Rhomboclase SPT139
SiO_2 (wt. %)	1.14	4.39	2.6	0.48
TiO_2 (wt. %)	0.09	0.06	0.04	0.04
Al_2O_3 (wt. %)	1.25	2.01	0.21	0.02
Fe_2O_3[b] (tot.) (wt. %)	(94.05)	(27.01)	(95.02)	(98.24)
FeO[c] (wt. %)	0.34	0.00	0.00	0.28
Fe_2O_3[c] (wt. %)	93.67	27.01	95.02	97.93
MnO (wt. %)	0.08	0.01	0.04	0.01
MgO (wt. %)	1.34	0.27	0.31	0.02
CaO (wt. %)	0.34	0.41	0.7	0.22
Na_2O (wt. %)	0.44	4.25	0.58	0.08
K_2O (wt. %)	0.04	1.69	0.1	0.01
P_2O_5 (wt. %)	0.04	0.07	0.03	0.01
SO_3 (wt. %)		33.16		
Total	99.77[d]	99.16	99.63[d]	99.63[d]
LOI[e]	71.45	58.99	63.22	74.79
SO_3[f]	31.10		35.38	26.87
H_2O[g]	40.35	25.83	27.84	47.92
Sr (ppm)	6	<5	15	<2
Zr (ppm)	<1	15	29	10
V (ppm)	13	90	72	<1
Co (ppm)			<2	
Cr (ppm)	8	55	48	21
Ni (ppm)			<2	
Rb (ppm)			8	
Pb (ppm)	65			5
Zn (ppm)	2345			33
XRD[h]	coquimbite, paracoquimbite	ferricopiapite, minor jarosite	fibroferrite, minor butlerite	pure rhomboclase

[a]Analyzed by X-ray fluorescence at Franklin and Marshall College by Stan Mertzman (March 2002).
[b]Total Fe expressed as Fe_2O_3.
[c]FeO determined by wet chemistry and Fe_2O_3 as difference between total Fe and FeO.
[d]Elemental totals expressed on a volatile-free basis.
[e]Loss on ignition represents percent weight loss after heating to 900°C for 1 to 1.5 h.
[f]S expressed as SO_3 and determined by ignition at the University of Alberta (August 2000).
[g]H_2O is taken as the difference between the measured values of LOI and SO_3.
[h]Phases listed in order of abundance as measured by X-ray diffraction at the University of Manitoba Department of Geological Sciences in May and June of 1999. The samples were run in continuous scanning mode to provide information on the <45 μm size samples and whether any accessory phases are present.

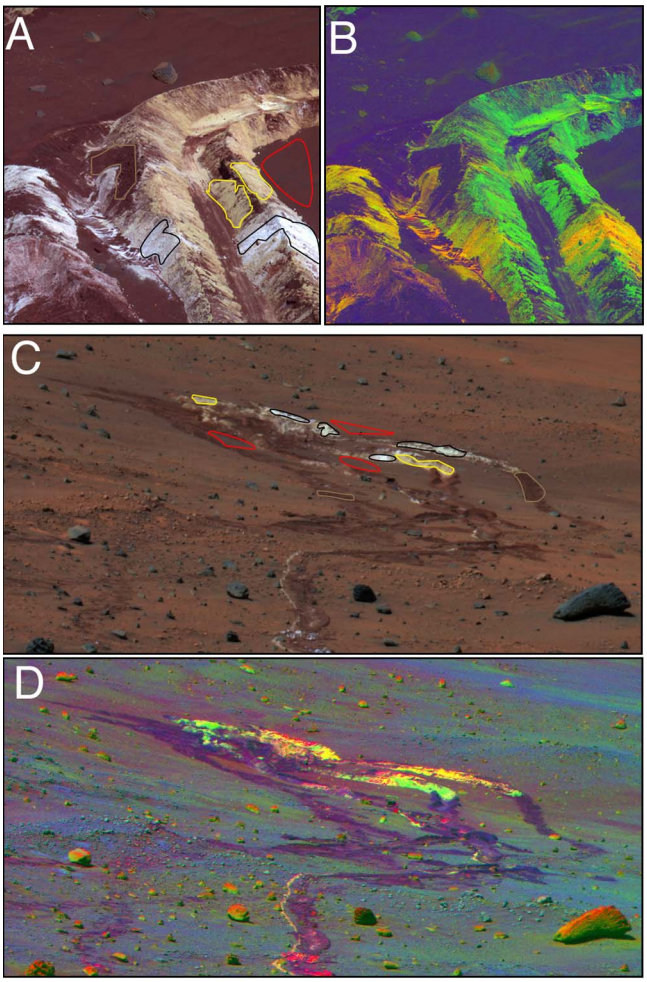

Figure 2. Pancam image products of the Tyrone soil exposure: (a) false color composite (blue, 432 nm; green, 535 nm; red, 753 nm) and (b) decorrelation stretch (DCS) image (made from 432 nm, 535 nm, and 753 nm filter images) from sol 790 (P2531); field of view is ~65 cm. (c) False color composite and (d) DCS image from sol 864 (P2547); wheel tracks are ~16 cm wide. Regions of interest (ROIs) from which spectra were acquired are enclosed by black, yellow, red, and brown lines for the white and yellow soil hues, undisturbed soil, and dark disturbed soil, respectively.

first month, and then on a roughly monthly basis (9 spectra acquired over 150 days of exposure). In every case, 1000 spectra of the dark current, standard and sample were acquired to provide sufficient signal to noise for subsequent interpretation.

[28] During the experiment, the ferric sulfate samples exhibited various decreases in volume that resulted in sample surface shrinkage, the sample moving away from the sides of the well, and/or cracking. When coupled with the small path length of the ASD probe to the sample, the surface shrinkage sometimes caused a significant change in overall reflectance. Because the samples could not be accessed during the experimental run, we chose to analyze the results as scaled reflectance (all spectra normalized to unity at 1250 nm), rather than in absolute reflectance. We note that normalizing the spectra has no effect on the calculated values of the spectral parameters used in this study, which are all based on relative, rather than absolute, reflectance levels.

[29] To simulate MER Pancam observations of these minerals on the Martian surface, we multiplied the high-resolution laboratory spectra by the solar spectrum, weighted the resulting radiance spectra by the Pancam spectral bands (Table 1) [*Bell et al.*, 2003], and divided the radiance value at each band by the solar spectrum weighted by that band. This method provides 11 wavelength spectra that we can use for direct comparison with Pancam spectra in R^* values (see section 2.2.1 for an explanation of R^*). From each weighted spectrum, we calculated the values of the three spectral parameters described in section 2.1.3 that characterize distinctive regions of the Vis-NIR spectra of ferric sulfates (Table 3): (1) the 753 to 432 nm ratio; (2) the 535 nm band depth; and (3) the 864 nm band depth. We use the observed changes to these spectral parameters as predictors of how the Pancam instrument would detect spectral changes due to the dehydration of ferric sulfate soils on the Martian surface. Laboratory spectra were also weighted by the three HiRISE band passes [*Delamere et al.*, 2010] using the same procedure described above.

3. Observations of Spectral Variations

3.1. Pancam Observations

3.1.1. Tyrone Soil Exposure

[30] The Tyrone bright soil was excavated by Spirit's wheels on sol 782, after which the rover became temporarily stuck in the fine, unconsolidated materials. During the extraction process, Spirit's inoperative right front wheel exhumed yellow-hued soils from depths of ~11 cm, which appear to be segregated below the white-hued soils that are found in the shallower left wheel trench (Figure 2) [*Wang et al.*, 2008]. One Pancam 13-filter image sequence was acquired of the soils at the Tyrone site on sol 790, after which Spirit was directed to Low Ridge to park with a northerly tilt for the winter (Figure 1). From a distance of ~30 m, the team periodically imaged the Tyrone exposure, acquiring five images from sols 864 to 1005 (Table 2). We note that one additional Pancam 13-filter observation was acquired from Low Ridge on sol 856 (P2297), but because this observation is part of the larger McMurdo 360° panorama and the Tyrone exposure is located at the seam between two frames, and because six of the thirteen filter images have saturated pixels, we omit this observation from our analysis. At the end of its winter campaign, the team acquired two additional full filter images of Tyrone on sols 1036 and 1062 as Spirit resumed its traverse.

[31] We use decorrelation stretch (DCS) images [*Gillespie et al.*, 1986] made from L7 (432 nm), L5 (535 nm) and L2 (753 nm) filter images to enhance the color variations within each scene and to identify spectral separations within the soil exposure (Figures 2b and 2d). Two hues are distinct within the Tyrone bright soil exposure, even in the observations acquired from ~30 m distance at Low Ridge: (1) the "white" soil (yellow in DCS images); and (2) the "yellow" soil (green in DCS images). Spectra of the "white" and "yellow" soil hue separations, in addition to spectra of undisturbed surface soil and disturbed, dark soil within the

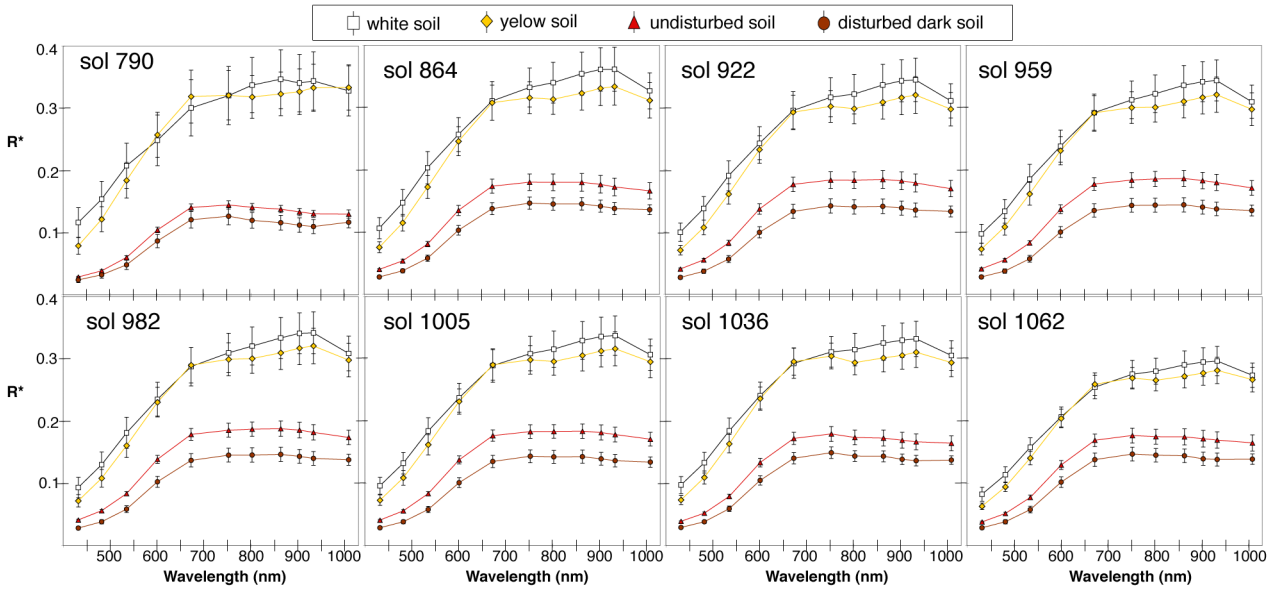

Figure 3. Pancam spectra from the eight 13-filter Tyrone observations: sol 790, sol 864, sol 922, sol 959, sol 982, sol 1005, sol 1036, and sol 1062 (Table 2). The "white" and "yellow" soils, undisturbed soil, and dark disturbed soil are shown as white boxes, yellow diamonds, red triangles, and brown circles, respectively.

wheel tracks, are shown for each of the eight Pancam observations in Figure 3. As noted in previous studies, the "yellow" spectrum is characterized by a steep blue-to-red spectral slope and a minor absorption near 800–864 nm consistent with ferric sulfate minerals, while the "white" spectrum typically exhibits higher reflectance values at all wavelengths and a 934 to 1009 nm ratio greater than unity [*Johnson et al.*, 2007; *Wang et al.*, 2008; *Lane et al.*, 2008; *Parente et al.*, 2009; *Rice et al.*, 2010a].

[32] Of the eight full spectral observations at Tyrone, the largest temporal changes occur between the sol 790 and sol 864 observations, where the reflectance maximum of the yellow hue at 670 nm decreases relative to the white hue (Figure 3). An increase in the 934 to 1009 nm ratio also appears between these sols in the "yellow" spectrum. We note that because of differences in viewing geometry (emission angle difference of 22.7°; Table 2) and resolution (0.06 cm/pixel and 0.7 cm/pixel), the spectra from these two observations were not extracted from the exact same regions of the soil exposure or CCD image frame region (Figure 2). The five observations acquired between sols 864 and 1005 were acquired from the same position, however, and the sol 1036 and sol 1062 observations were acquired from a similar distance (~30 m) after short drives. Spectral comparisons of these last seven observations are therefore significantly more straightforward than comparisons between the first two observations.

[33] The left column of Figure 4 shows the values of the 535 nm band depth, 734 to 432 nm ratio, 864 nm band depth and 934 to 1009 nm ratio for each observation. Variations in these spectral parameters for the white and yellow soil hue separations are often paralleled by variations in the undisturbed and dark disturbed soils, suggesting that some changes reflect systematic differences between entire images (such as air fall dust accumulation, or changes in viewing geometry and illumination angle; Table 3), rather than variations from region-to-region within individual images. To account for such image-to-image variations, we divide the spectral parameters of the bright soils by those of undisturbed soils in the same image, which we assume do not vary with time. Plots of these ratios versus sol are shown in the right column of Figure 4. As ratios, the 535 nm band depths of the yellow and white soil hues increase 50–200% between sols 790 and 959, and 66–68% between sols 1005 and 1062; these variations are the same magnitude as the statistical errors shown in Figure 4b.

[34] The most significant change in the spectra of the yellow and white soil hues relative to undisturbed soils is seen in the red to blue (753 to 432 nm) ratio between sols 790 and 864 (Figure 4d). The 26% and 15% changes to the white soil and yellow soil, respectively, represent a "reddening" of both materials over 74 sols that is larger than the size of the statistical errors. No statistically significant variations are observed in the bright soils relative to the dusty undisturbed soil in the 753 to 432 nm ratio after sol 864, nor in the 864 nm band depth, nor the 934 to 1009 nm ratio over all sols. The increase in the 934 to 1009 nm ratio for the yellow hue between sols 790 and 864, noted above and seen in Figure 3, falls within the range of statistical errors shown in Figure 4h.

[35] For the five observations acquired from the same position (sols 864 to 1005), we have performed a pixel-to-pixel analysis to complement the image-based analysis discussed above. Our derived percent change maps (Figure 5; percent change maps are described in section 2.1.5) highlight regions where spectral parameters are increasing (or decreasing) with time as bright (or dark) relative to the rest of the map. In the 535 nm band depth percent change map (Figure 5a), the Tyrone soil is brighter than surrounding materials, indicating that the 535 nm band depth increases

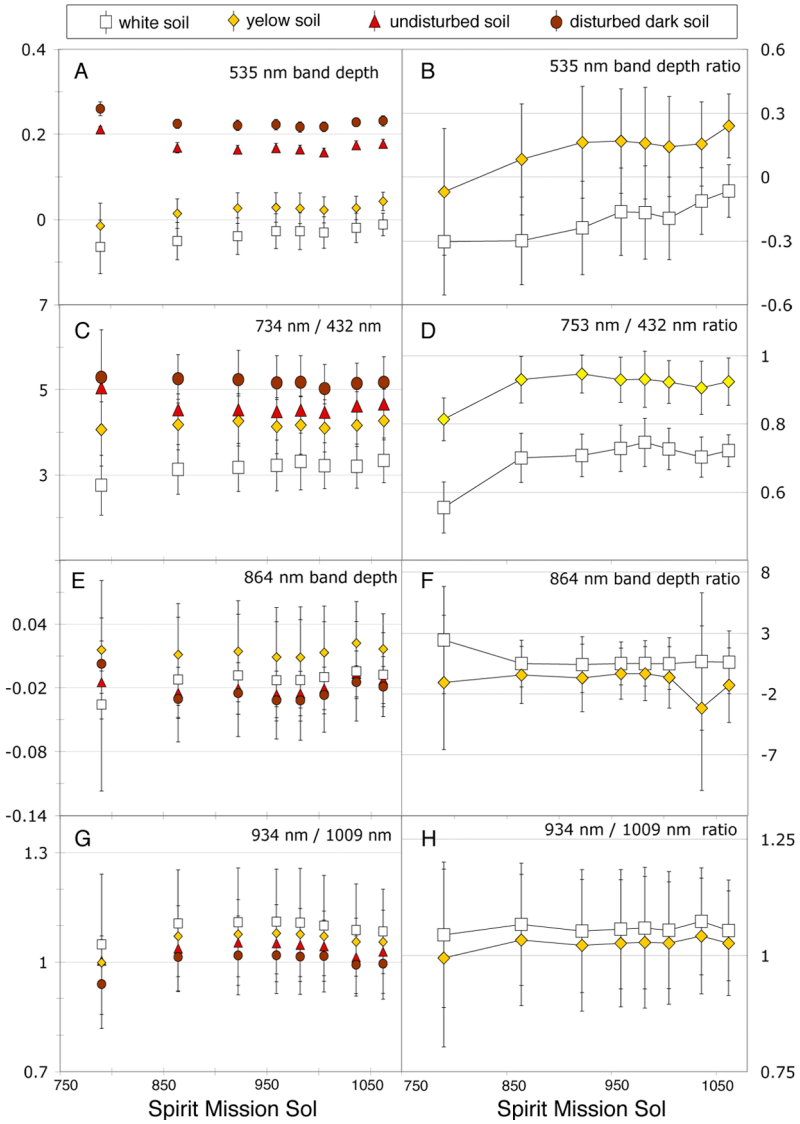

Figure 4. Pancam spectral parameters (Table 3) of the Tyrone "white" (white boxes) and "yellow" (yellow diamonds) soils, undisturbed soil (red triangles), and disturbed dark soil (brown circles) displayed as (left) absolute values and (right) the ratios of the "white" and "yellow" soils to undisturbed soil: (a–b) 535 nm band depth, (c–d) 753 to 432 nm ratio, (e–f) 864 nm band depth ratio, and (g–h) 934 to 1009 nm ratio. Regions of interest (ROIs) from which spectra were acquired are shown in Figure 2.

systematically over the five observations. The average increase for the white and yellow Tyrone soil pixels is 120%. We note that dark, basaltic rocks also exhibit trends of increasing in 535 nm band depth with time (up to 100% increase). Portions of the Tyrone soil are also brighter than surrounding materials in percent change maps of the 753 to 432 nm ratio (Figure 5b); the average change for the white soil is an increase of 4%, and the yellow soil is a decrease of 2%. The variability of percent change values among neighboring pixels is large, as the standard deviations of the white and yellow soil values are 6–7%. Percent change maps for the 864 nm band depth and 934 to 1009 nm ratio show no changes at the Tyrone soil relative to surrounding materials (Figures 5c–5d). Interpretations of these observations are discussed in section 5.

3.1.2. Gertrude Weise Soil Exposure

[36] The silica-rich Gertrude Weise soil was exposed by Spirit's inoperative right front wheel on sol 1148 and Pancam full filter observations were acquired on sols 1158, 1187 and 1198 (Table 2). Because the three observations were acquired from different viewing geometries (Figure 6), they could not be coregistered for pixel-to-pixel comparisons. DCS images of Gertrude Weise reveal that, unlike the Tyrone exposure, the Gertrude Weise trench is spectrally homogeneous and only has one hue (right column of Figure 6); however, the shallower Lefty Ganote trench, exhumed by Spirit's left wheels and also visible in Figure 6, contains a mixture of silica-rich and basaltic soils and exhibits a range of hues. Spectra from the three Pancam observations are nearly identical (Figure 7), and are characterized by a steep slope

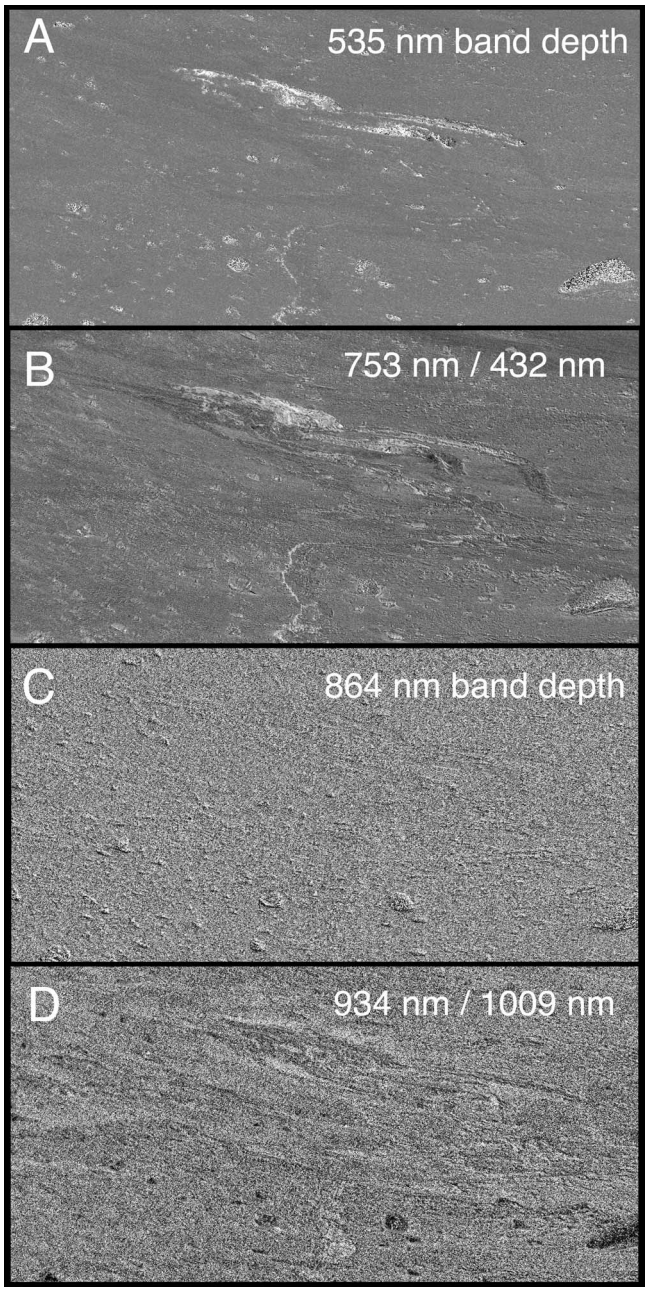

Figure 5. Percent change maps calculated from a linear regression fit to spectral parameter versus sol data for the Pancam observations of Tyrone from sols 864 to 1005. Bright pixels indicate an overall increase of the spectral parameter with time; darker pixels correspond to an overall decrease of the spectral parameter with time: (a) 535 nm band depth (black corresponds to <−100%, white to >100%), (b) 753 nm/432 nm (black corresponds to <−15%, white to >15%), (c) 864 nm band depth (black corresponds to <−15%, white to >15%), and (d) 934 nm/1009 nm (black corresponds to <−15%, white to >15%). False color and DCS images of this scene are shown in Figures 2c–2d.

from 432 nm to 864 nm, a flat near-infrared profile from 864 nm to 934 nm, and a steeply negative slope from 934 nm to 1009 nm [*Wang et al.*, 2008; *Rice et al.*, 2010a]. The spectral parameters measured for the white soil (535 nm band depth, 753 nm to 432 nm ratio, 864 nm band depth and 934 nm to 1009 nm) vary slightly between observations, but when measured relative to undisturbed soil, we observe no statistically significant changes to any parameter (Figure 8).

3.1.3. Kit Carson Soil Exposure

[37] Spirit's right front wheel exposed the bright Kit Carson soil on sol 1861, and Pancam acquired two observations on sols 1864 and 1866 as Spirit continued its traverse south (Table 2). Because a drive occurred between the two

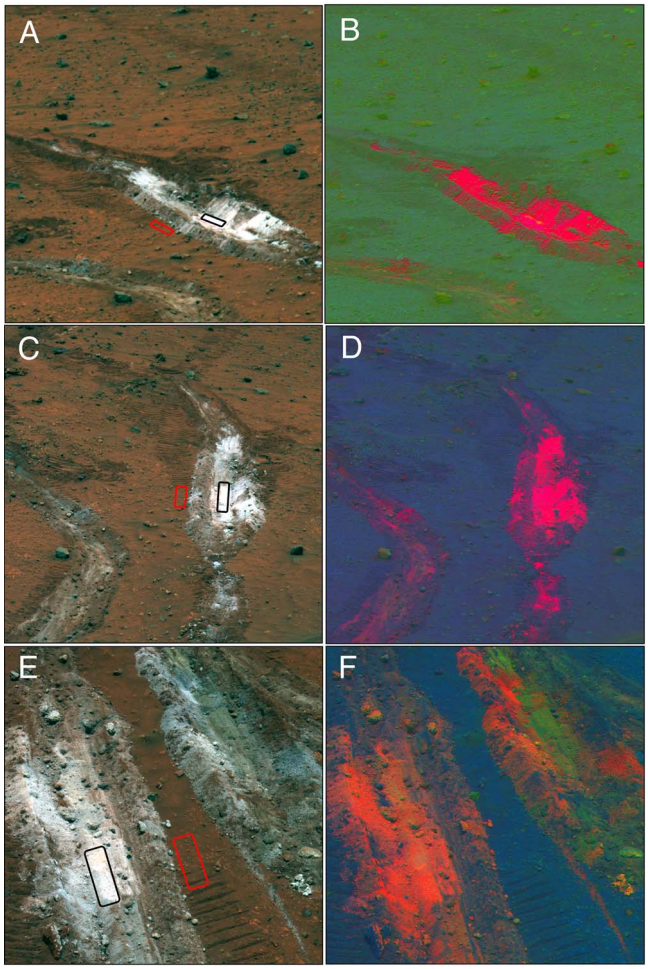

Figure 6. Pancam image products of the Gertrude Weise soil exposure (the rover's right wheel trench with ROIs outlined is Gertrude Weise; the rover's left wheel trench is Lefty Ganote, which is not considered in this study): (a) false color composite (blue, 432 nm; green, 535 nm; red, 753 nm) and (b) decorrelation stretch (DCS) image (made from 432 nm, 535 nm, and 753 nm filter images) from sol 1158 (P2581). (c) False color composite and (d) DCS image from sol 1187 (P2533). (e) False color composite and (f) DCS image from sol 1198 (P2539). Wheel tracks are ~16 cm wide. Regions of interest (ROIs) from which spectra were acquired are enclosed by black and red boxes for the white soil hue and relatively undisturbed soil, respectively.

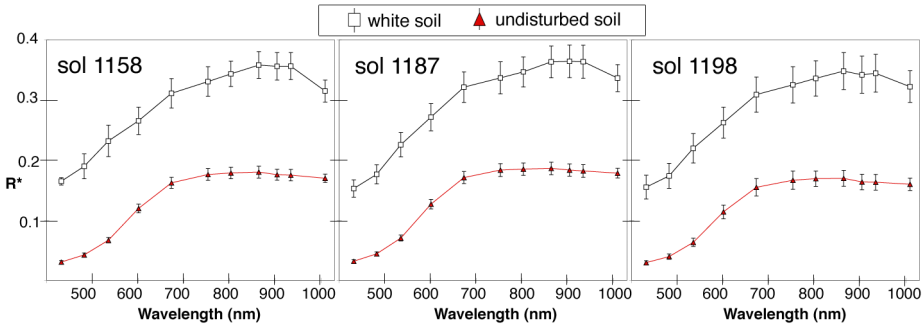

Figure 7. Pancam spectra from the three 13-filter Tyrone observations: sol 1158, sol 1187, and sol 1198. The "white" soil and undisturbed soil are shown as white boxes and red triangles, respectively.

observations, there is a limited region of overlap for comparison between the two images (Figures 9a–9b, bottom right, and Figures 9c–9d, top left). Spectra from the two observations were thus acquired from ROIs in different regions of the FOV, and are variably affected by the dust contamination described in section 2.1.4.

[38] In false color and DCS images (Figure 9), two color hue separations are visible within the trench, similar to those

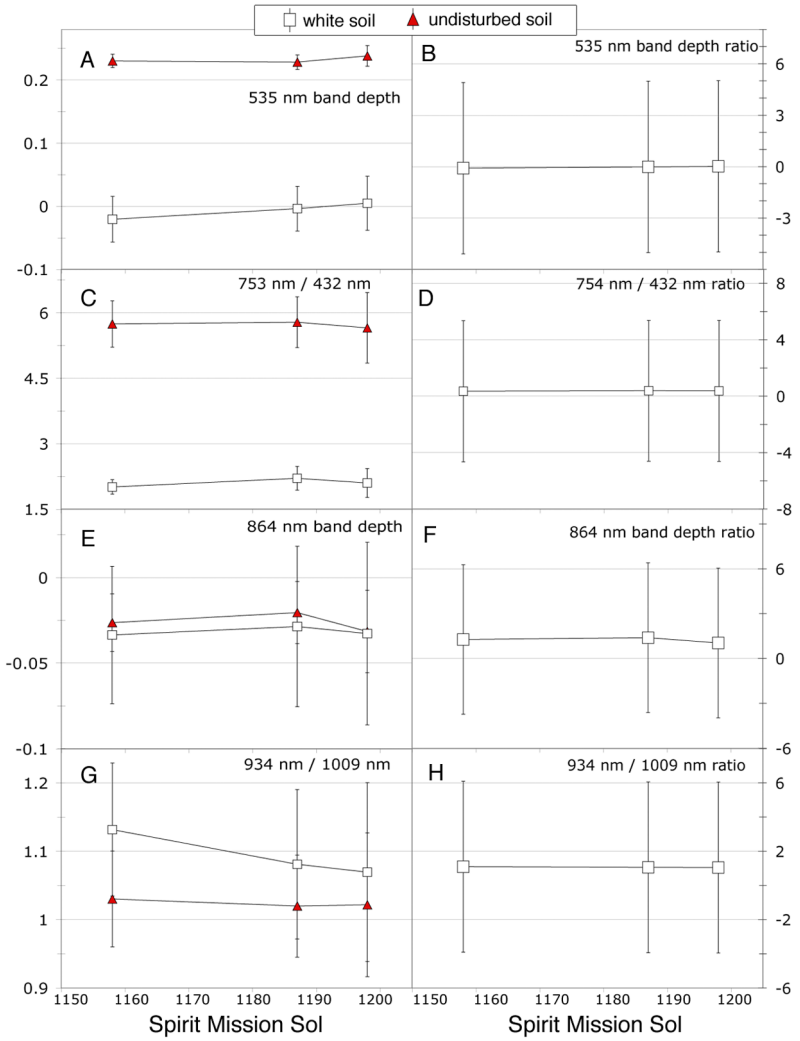

Figure 8. Pancam spectral parameters of the Gertrude Weise soil (white boxes) and undisturbed soil (red triangles) displayed as (left) absolute values and (right) the ratios of the "white" soil to undisturbed soil: (a–b) 535 nm band depth, (c–d) 753 to 432 nm ratio, (e–f) 864 nm band depth, and (g–h) 934 to 1009 nm ratio.

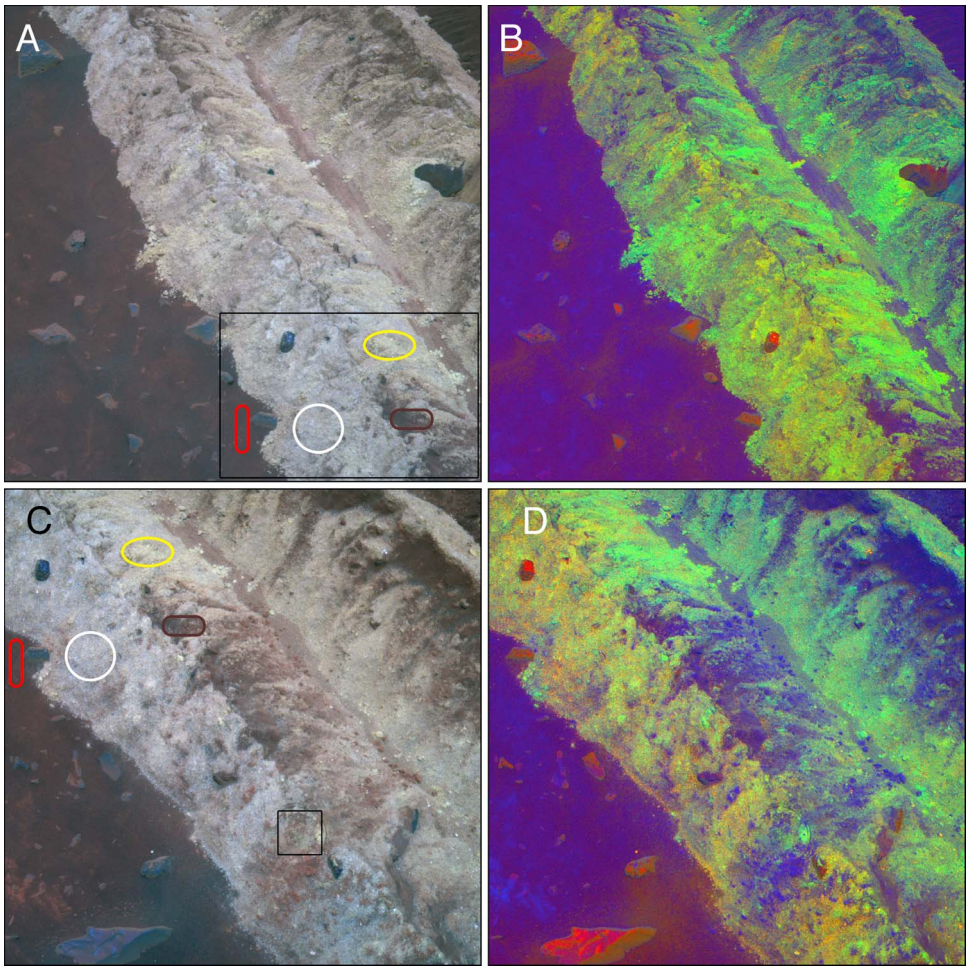

Figure 9. Pancam image products of the Kit Carson soil exposure: (a) false color composite (blue, 432 nm; green, 535 nm; red, 753 nm) and (b) decorrelation stretch (DCS) image (made from 432 nm, 535 nm and 753 nm filter images) from sol 1864 (P2562), field of view is ~50 cm. (c) False color composite and (d) DCS image from sol 1866 (P2555), field of view is ~37 cm. Regions of interest (ROIs) from which spectra were acquired are enclosed by white, yellow, red, and brown ovals for the white and yellow soil hues, undisturbed soil, and dark disturbed soil, respectively. The black box in Figure 9a indicates the location of Figure 20a; the black box in Figure 9b indicates the location for Figure 21.

observed at the Tyrone exposure: (1) "white" soil (yellow in DCS images) and (2) "yellow" soil (green in DCS images). Spectra of these two hue separations, dark disturbed soil and undisturbed soil are shown in Figure 10. The observations from sol 1864 contain a reduced filter set due to limited time and power resources, so we cannot compute the 535 nm band depth for this observation as defined in Table 3. Observed changes to the bright soils include an increase in reflectance of dark disturbed soil, an increase in 864 nm band depth and increase in 753 nm to 432 nm ratio between sols 1864 and 1866 (Figure 10). Figures 11a and 11c show that increases in the 753 nm to 432 nm ratio and 864 nm band depth for the white and yellow soils are mirrored by changes in the dark and undisturbed soils in the same portion of the image, and the 753 nm to 432 nm ratio and 943 nm to 1009 nm ratios for the bright soils do not change relative to the undisturbed soil (Figures 11b and 11f). The 864 nm band depth does increase relative to surrounding materials, however, by >200% for both the yellow and white

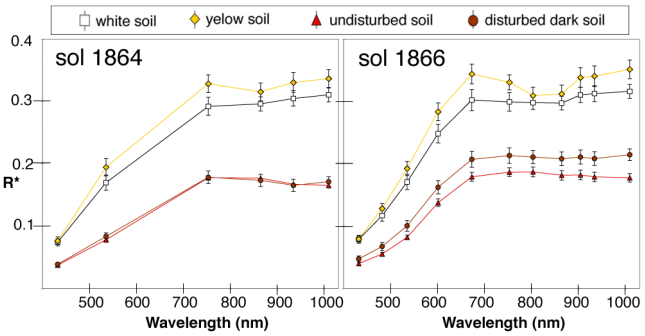

Figure 10. Pancam spectra from the 8-filter (sol 1864, P2562) and the 13-filter (sol 1866, P2555) observations of Kit Carson. The "white" and "yellow" soils, undisturbed soil, and dark disturbed soil are shown as white boxes, yellow diamonds, red triangles, and brown circles, respectively. Spectra were extracted form the regions of interest (ROIs) shown in Figure 13.

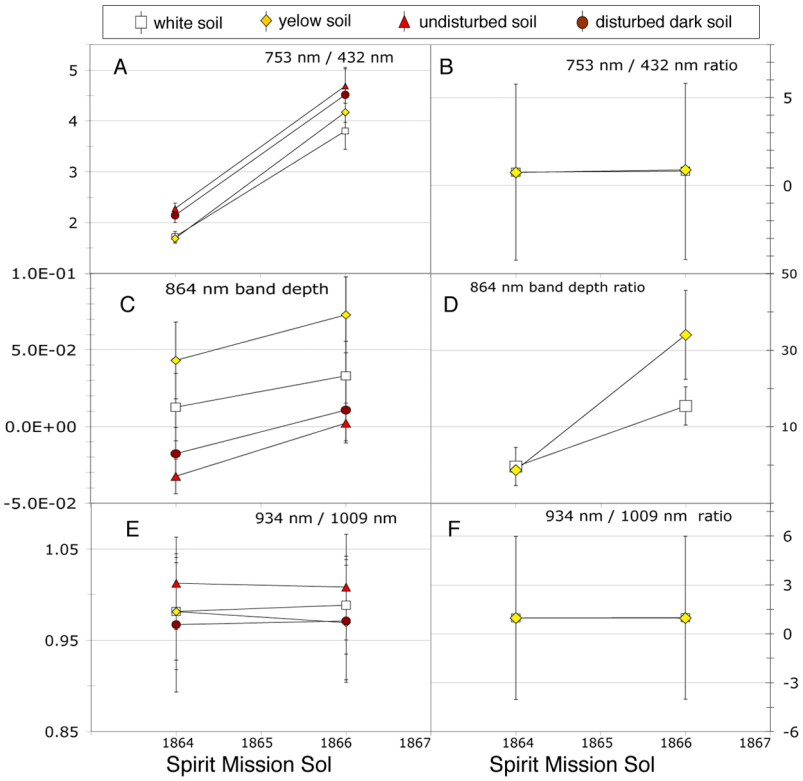

Figure 11. Pancam spectral parameters of the Kit Carson "white" (white boxes) and "yellow" (yellow diamonds) soils, undisturbed soil (red triangles), and disturbed dark soil (brown circles) displayed as (left) absolute values and (right) the ratios of the "white" and "yellow" soils to undisturbed soil: (a–b) 753 to 432 nm ratio, (c–d) 864 nm band depth, and (e–f) 934 to 1009 nm ratio.

soil hues (Figure 11d). This observation implies that there is still a statistically significant increase in band depth even when we account for systematic image-to-image variations; possible causes of this change are discussed in section 5.

3.1.4. Ulysses Soil Exposure

[39] The Ulysses bright soil was exposed during Spirit's drive south from Kit Carson on sol 1886, when the rover became stuck in the fine-grained, unconsolidated material. Seven full filter Pancam observations of the exposure were acquired between sols 1888 and 2019 (Table 2). Three additional 13-filter subframes were acquired within the trench on sols 1901–3, but because these observations were acquired at high phase angles on only a small portion of the soil exposure, we do not include them in our analysis. During the extrication efforts, the rover changed position slightly between each Pancam observation until sol 1933 (Table 2), and we have been careful to select ROIs for our spectral analysis that are visible in each of the seven observations and that have not been further disturbed by the extrication activity (Figure 12). A detailed description of the measurement campaign at Ulysses with Spirit's full suite of instruments has been provided by *Arvidson et al.* [2010].

[40] False color and DCS images from the first Pancam observation on sol 1888 reveal two color hue separations within the trench (Figures 12a–12b), as observed at the Kit Carson and Tyrone exposures: (1) "white" soil (yellow/red in DCS images) and (2) "yellow" soil (green in DCS images). By sol 1982, the color of the Ulysses soil had visibly changed (Figure 12c), and the two hues are no longer distinguishable in DCS images (Figure 12d). These changes are reflected in the spectra shown in Figure 13, where the "yellow" and "white" spectra, as well as the dark disturbed soil spectra, have converged to the same shape in the sol 1933–2019 observations; the negative 934 nm to 1009 nm slope characteristic of the "white" spectrum has flattened, and all spectra develop a reflectance maximum at 904 nm. We note that spectra from the Ulysses imaging campaign were acquired from a wider range of incidence angles than other campaigns (Table 2), which results in the variability in overall reflectance between observations for all surface materials, most notably with the sol 2019 observation (Figure 13). In this study, however, we are concerned with changes to relative spectral features rather than changes in absolute reflectance.

[41] Over the first nine sols of observation, the most significant change to the bright soils relative to the undisturbed soil is an increase in the 753 nm to 432 nm ratio for the white soil (Figure 14d). After sol 1897, the 934 to 1009 nm ratio does not change over the observation period (Figure 14h), but all other parameters vary considerably. By sol 2019, the 535 nm band depth, 753 to 432 nm ratio and 864 nm band depth of the bright soils approach the values for the dark disturbed surface soils (Figures 14a–14f). Interpretations of these changes are provided in section 5.

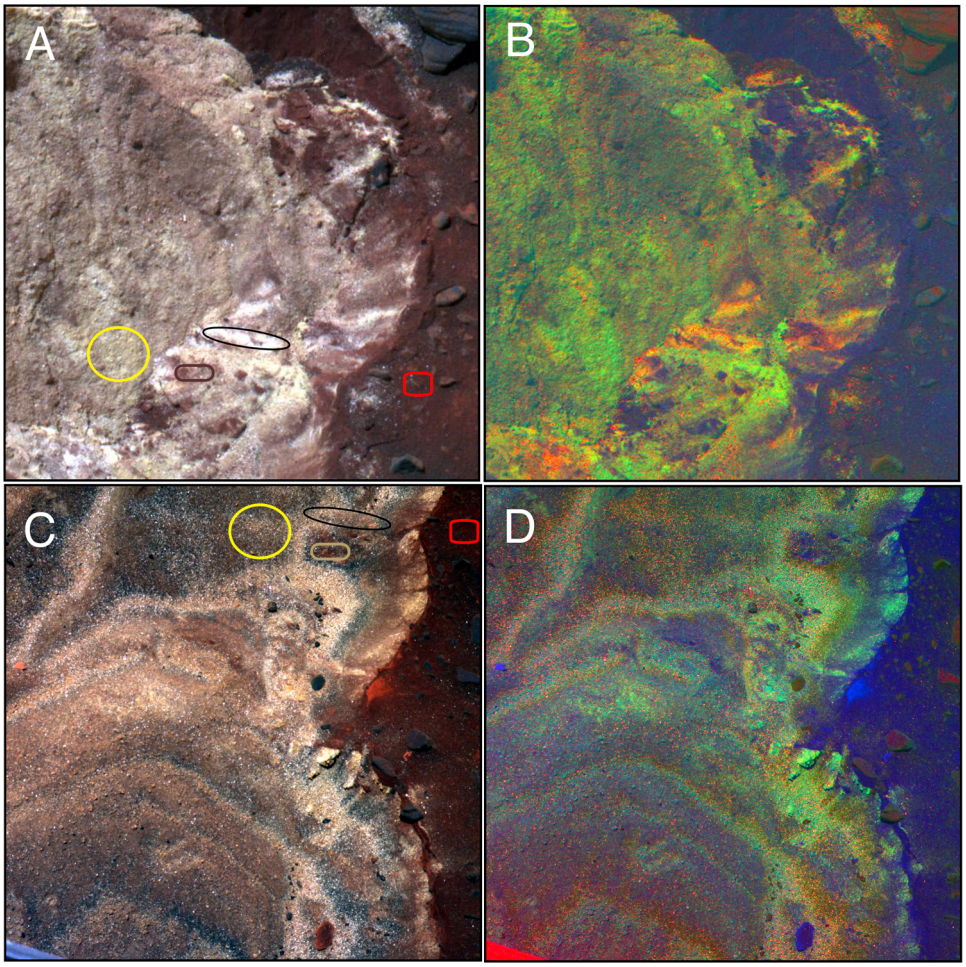

Figure 12. Pancam image products of the Ulysses soil exposure: (a) false color composite (blue,432 nm; green, 535 nm; red, 753 nm) and (b) decorrelation stretch (DCS) image (made from 432 nm, 535 nm, and 753 nm filter images) from sol 1888 (P2559), field of view is ~24 cm. (c) False color composite and (d) DCS image from sol 1982 (P2547), field of view is ~34 cm. Regions of interest (ROIs) from which spectra were acquired are enclosed by white, yellow, red, and brown ovals for the white and yellow soil hues, undisturbed soil, and dark disturbed soil, respectively.

3.2. HiRISE Observations

[42] The Kit Carson soils were exposed on sol 1861, and a HiRISE image acquired 20 sols later demonstrated that they could be seen from orbit in the RED filter (Figure 15a). A follow-up HiRISE imaging campaign was planned, including two three-color images on sols 1935 and 1967 (Table 4 and Figure 15b); another image acquired on sol 1994 (ESP_014277_1650) provides additional coverage, but at lower resolution and only in the RED filter. Shortly thereafter, MRO entered an extended "safe mode" period during which all science instruments were powered off, preventing acquisition of additional images. A significant regional dust storm also occurred in Gusev crater during this period, with atmospheric opacity peaking at $\tau > 2.6$ on sol 2007 and subsequent dust settling on the surface (as measured by the reduced power output of Spirit's solar panels; Figure 25 and *Arvidson et al.* [2010]). Six months later, in the first HiRISE image acquired after MRO exited safe mode, Kit Carson and other bright soils were no longer visible in any filters (Figure 15c). Our change detection campaign is therefore limited to the two color images listed in Table 4.

[43] Between sols 1935 and 1967, our four calibration outcrops (labeled "cal" 1–4 in Figure 15) exhibited relative brightening of 2–4% in BG, 3–5% in RED, and 2–3% in the IR (relative I/F measurements for cal 2 and cal 4 are shown in Figures 16e–16f). We calculated relative I/F values for two spots within the Kit Carson exposure (labeled as "west" and "north" in Figure 15b), Gertrude Weise, Tyrone, and four calibration outcrops using "Denominator 1" from Figure 15b. Using other denominators changed the results by 2% or less in all cases. Virtually all of the exposed soils and the calibration spots show similar spectral behavior: a relative brightening over 32 sols in the BG, IR and RED bands (by 4–10%, 1–4%, and 1–5%, respectively), with the exception of Tyrone and the Cal4 spot, which decrease in RED and/or IR (Figure 16, left). As ratios (Figure 16, right), IR/RED for the bright soils changes by −3% to 0.5% and RED/BG changes by −8% to −3%. All observed variations are within the size of the estimated instrumental errors.

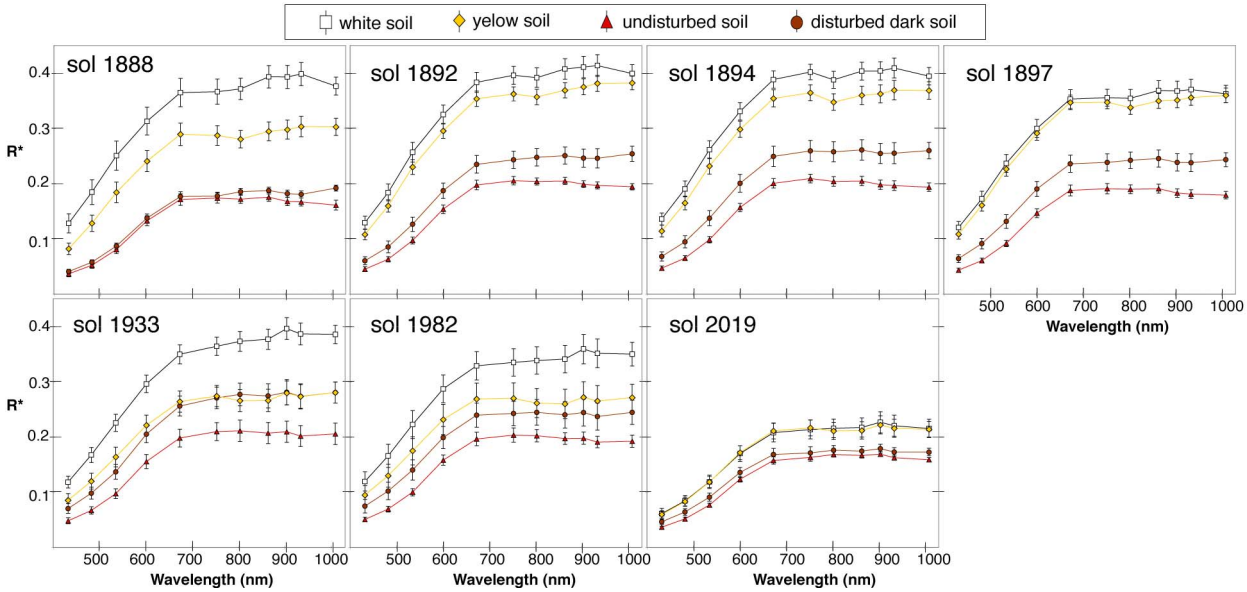

Figure 13. Pancam spectra from the seven 13-filter Ulysses observations: sol 1888, sol 1892, sol 1894, sol 1897, sol 1933, sol 1982, and sol 2019. The "white" and "yellow" soils, undisturbed soil, and dark disturbed soil are shown as white boxes, yellow diamonds, red triangles, and brown circles, respectively.

3.3. Laboratory Experiments

[44] Normalized spectra of coquimbite, ferricopiapite, fibroferrite and rhomboclase are shown in Figure 17 for days 1, 2, 24 and 125 of our laboratory experiment in a low-temperature and low-pressure environment. The major changes accompanying exposure to Mars surface conditions include changes in depth and wavelength position of OH and H_2O features at ~1400 nm and ~1900 nm, respectively (Figure 17a). These changes reflect differential loss of OH versus H_2O or OH/H_2O located in multiple sites [e.g., *Cloutis et al.*, 2008]. Changes in the visible region, which Pancam samples, can also be dramatic. For example, the ~430 nm Fe^{3+} band deepens in the coquimbite, ferricopiapite and fibroferrite spectra, and the ~790–900 nm Fe^{3+} features become less distinct for all samples. These spectral changes are linked to either a loss of H_2O and/or OH or a structural rearrangement of the OH that bridges between adjacent ferric irons [*Cloutis et al.*, 2008]. The modifications to the position and shape of the ~1.9 μm feature in the fibroferrite spectra further indicate a loss of H_2O and structural rearrangement.

[45] In Pancam band passes (Figure 17b), the effect of exposure to Martian conditions is primarily to decrease the contrast of spectral features. The changes to the Pancam spectral parameters listed in Table 3 are plotted against time in Figure 18 (excluding the 934 nm to 1009 nm ratio, which is an indicator of silica-rich materials, not ferric sulfates). Based on the observed trends, we predict that, if one or more of these candidate ferric sulfates are present in a bright soil deposit that is dehydrating upon exposure to surface conditions, the following changes could be observable in Pancam spectra: (1) an increase in the 535 nm band depth; (2) a decrease in the 753 to 432 nm ratio; and (3) a decrease in the 864 nm band depth. Because the spectral variations in Figure 18 reflect the samples equilibrating to Mars surface conditions from Earth surface conditions, whereas potential spectral variations observed by Spirit reflect an equilibration from Mars shallow subsurface conditions to a Mars surface condition, we do not predict the magnitude of possible Pancam spectral changes from our observations and consider only the direction.

[46] The HiRISE filters do not optimally sample the changes to the spectral features of ferric sulfates observed in Figure 17. The variations in the RED/BG and IR/RED ratios measured from the laboratory spectra weighted by the HiRISE band passes (Figure 19) are minor compared to the variations in the Pancam parameters observed over the 150 days of the experiment, exhibiting no changes greater than 5%. Thus we do not expect spectral changes due to the dehydration of coquimbite, ferricopiapite, fibroferrite or rhomboclase to be observed in HiRISE spectra.

4. Observations of Textural Variations

4.1. Kit Carson Soil Exposure

[47] Several textural modifications to the bright Kit Carson soil material are observed in the region of overlap between the sol 1864 and 1866 Pancam observations (Figure 20). The dragging motion of Spirit's inoperative right front wheel squeezed bright material out to either side of the trench, resulting in narrow, parallel ridges resembling levees composed of unconsolidated material at the angle of repose. The "white" and "yellow" soil hues have been mixed with dark soils and basaltic pebbles by the trench excavation. Figure 20 shows examples of the observed modifications to soil texture: partial disintegration of the soil clod in the bottom center of the image, and appearance of a "halo" of fine, bright material on undisturbed soil (Figure 20b); disappearance of bright material from small depressions in a rounded pebble (Figure 20c); appearance of fine, bright material in the dark

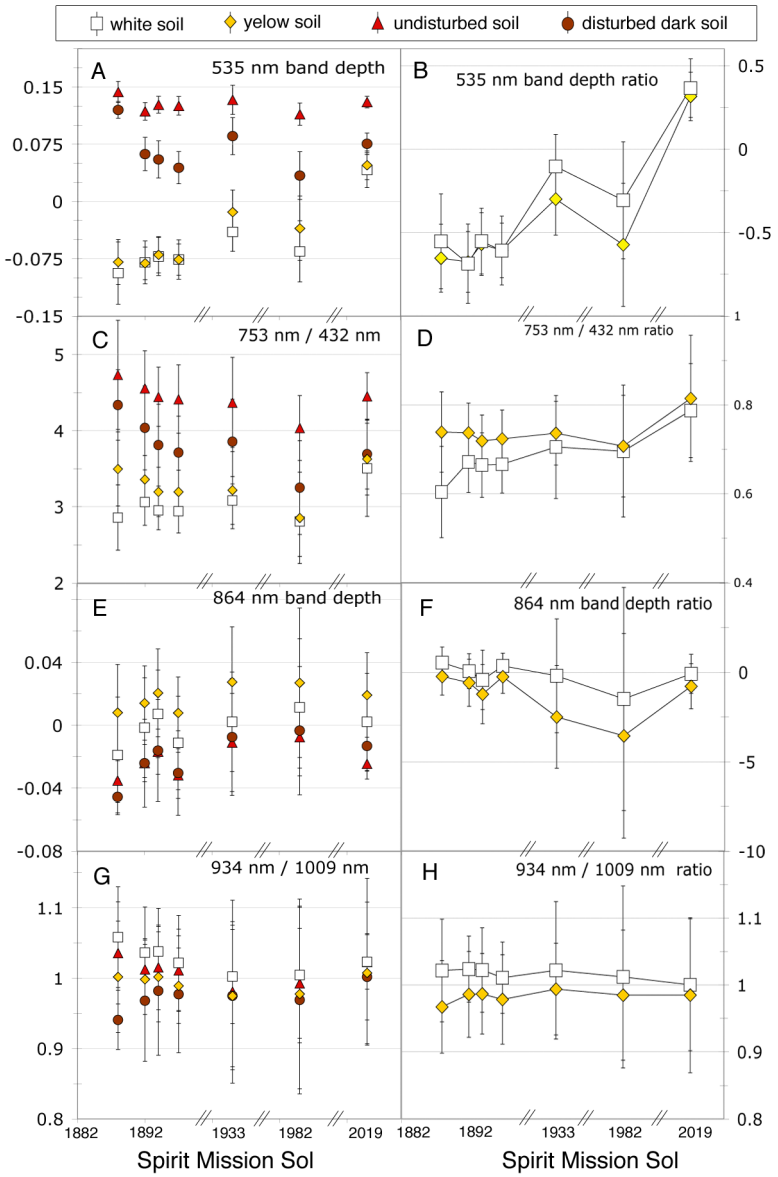

Figure 14. Pancam spectral parameters of the Ulysses "white" (white boxes) and "yellow" (yellow diamonds) soil hue separations, undisturbed soil (red triangles), and disturbed dark soil (brown circles) displayed as (left) absolute values and (right) the ratios of the "white" and "yellow" soils to undisturbed soil: (a–b) 535 nm band depth ratio, (c–d) 432 to 753 nm slope ratio, (e–f) 864 nm band depth ratio, and (g–h) 934 to 1009 nm slope ratio.

portion of wheel trench (Figure 20d); and modifications to small-scale topographic features within the trench (Figure 20e). Note that the two Pancam false color images are not at the same stretch, and these images should only be used for textural comparisons, not color comparisons (Figure 9).

[48] One MI observation of bright soil near the Kit Carson exposure was acquired on sol 1863 at the target called John Wesley Powell (Table 5; location shown in Figure 9); unfortunately, no additional MI observations were acquired at this site. A merge of this observation with Pancam false color is shown in Figure 21. The ring seen in this image is the impression of the Mössbauer (MB) contact plate, which had compressed the soil with a force of 1N. The soil in the MI observation is largely composed of 100–300 μm aggregates of grains smaller than the MI resolution limit. The "fluffy" aggregates are easily crushed by the MB contact, as seen by the dominance of <100 μm silt and fine-grained sand in the area compacted by the MB (Figure 21). The color variability in the image does not appear to correspond to any distinguishable textural variability among the color units.

4.2. Ulysses Soil Exposure

[49] Pancam observations reveal extensive textural changes within the Ulysses soil exposure over 131 sols. Figure 22 shows examples of the observed modifications: disappearance of fine bright material (Figure 22b); dispersal and removal of light material along the cliff at the eastern edge of

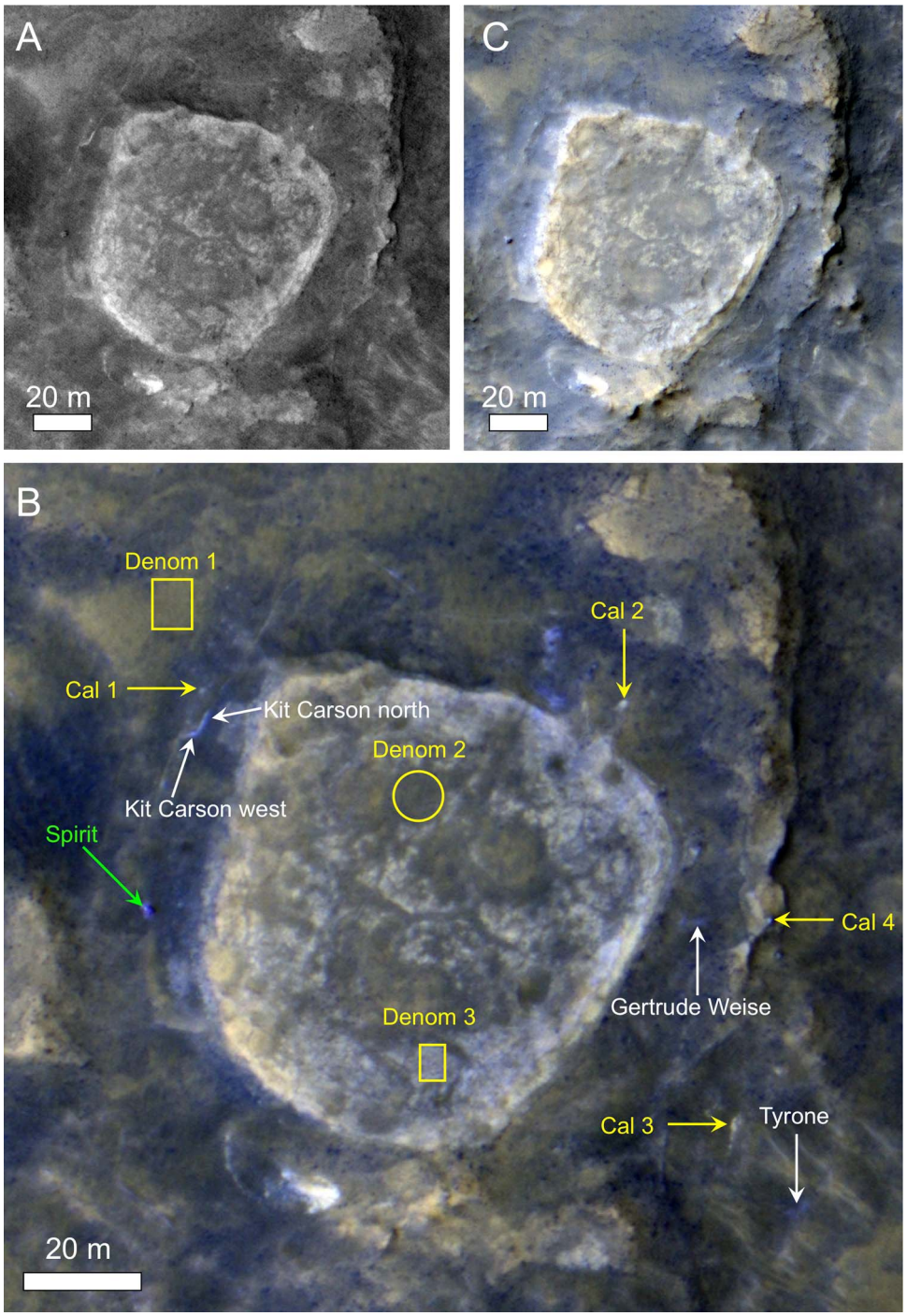

Figure 15. Orbital view of the region surrounding Home Plate in the Columbia Hills. (a) Portion of the first HiRISE image acquired after exposure of the Edgar Allen Poe and Kit Carson soils, ESP_012787_1650 (sol 1881). (b) "IRB" enhanced color composite [*McEwen et al.*, 2010] from ESP_013921_1650 (sol 1967); see section 5.3 for discussion. (c) IRB composite from ESP_016677_1650 (sol 2177), in which all bright soils are virtually invisible.

the exposure (Figure 22c); appearance of bright material along a cliff at the northern edge of the exposure (Figure 22d); and appearance of a bright soil clod (marked by the red circle) within the exposure (Figure 22e). The most dramatic changes to Figures 22b and 22c occur between sols 1897 and 1933, but some change is observed between each pair of observations. Within the bulk material, Pancam images show an increase in granularity with time as fine grained material appears to have been removed (Figure 12). The steep wall at the eastern edge of the exposure (Figure 22c) shows that the soil is weakly

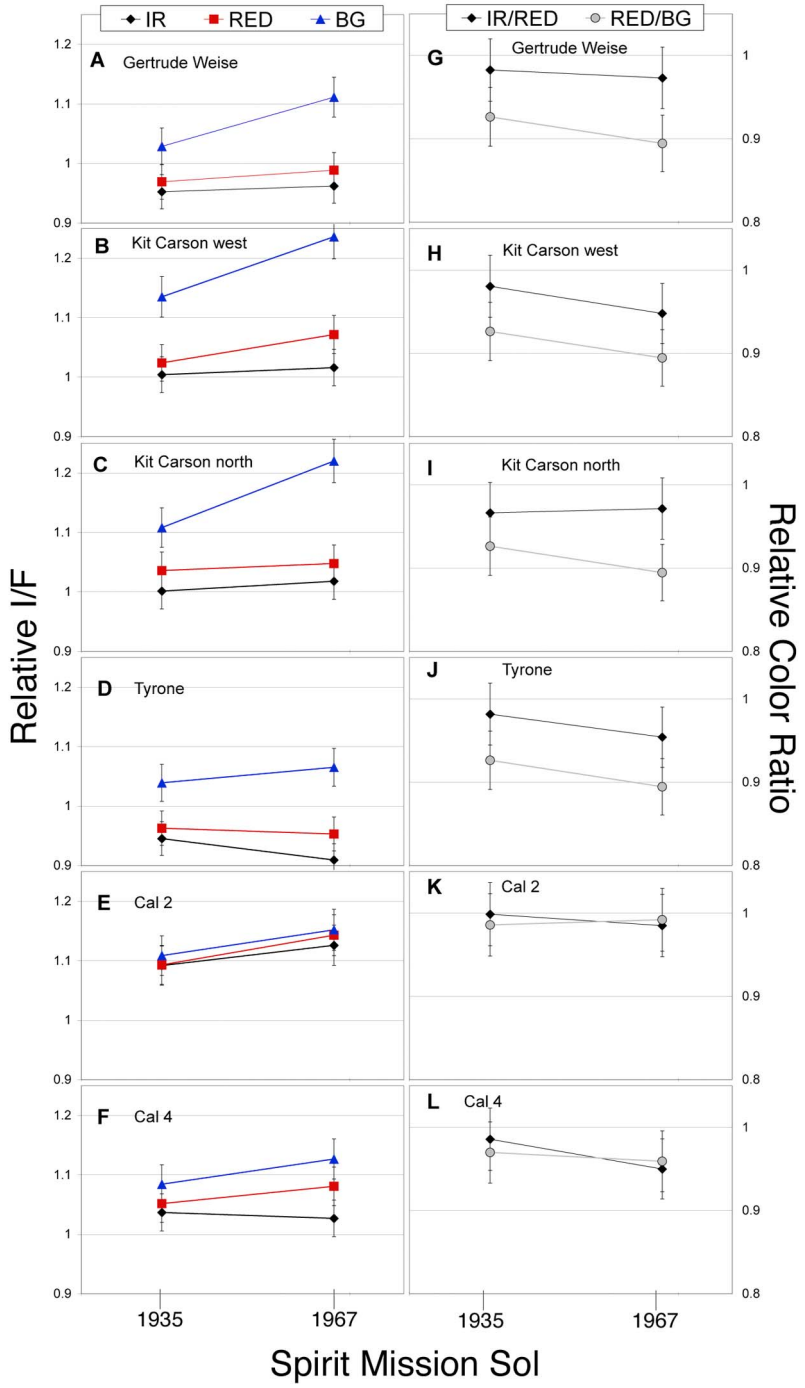

Figure 16. HiRISE spectral evolution of the Gertrude Weise, Kit Carson, and Tyrone bright soils from sols 1935 to 1967. Two example calibration outcrops (cal 2 and cal 4, locations indicated in Figure 15b) are shown for comparison. (left) Values are I/F for the three color filters of the feature of interest divided by that of a nearby undisturbed area (denom 1 in Figure 15b). (right) Values are color ratios (IR/RED and RED/BG) taken from the relative I/F values. Error bars are 2% of relative I/F.

cohesive at the surface, with cohesion seeming to decrease within the bulk bright soil material a few millimeters below the surface.

[50] Repeated MI observations within the Ulysses exposure were acquired at two targets called Penina (Figure 23) and Sackrider (Figure 24), locations of which are shown in Figure 22a. The four observations of Sackrider and three of Penina (Table 5) show that these targets are composed of angular, poorly sorted, sand-sized and finer particles (<300 μm), with some aggregates (mostly 500–700 μm) and a subpopulation of larger, rounded clasts (>800 μm). Most grains are opaque, but some grains that are bright or glinting

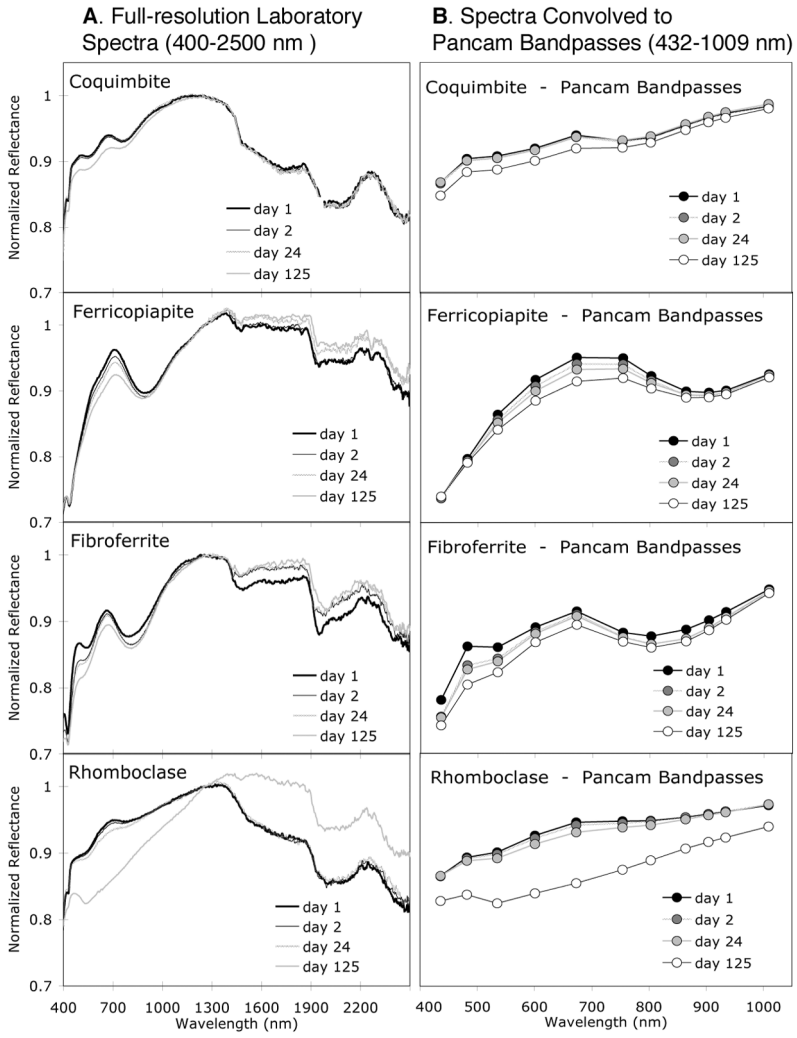

Figure 17. Spectra of ferric sulfate minerals (normalized to their value at 1250 nm) over the first 150 days of exposure to Martian surface conditions (P = 5 Torr CO_2; T = 20°C): (a) full resolution Vis-NIR spectra (400–2500 nm) and (b) spectra convolved to Pancam band passes. Spectra are shown for days 1, 2, 24, and 125 of the experiment; see text for experimental procedure.

are also observed (saturating the dynamic range of the MI camera). Some particles are two toned, and appear to be dark clasts coated by bright, fine-grained material [see also *Arvidson et al.*, 2010, Figures 13 and 17].

[51] At both Penina and Sackrider, a removal of fine-grained material is observed (Figures 23–24). We note that the first MI observation at Ulysses was acquired 36 days after the material was exposed, when the texture may already have been modified to some extent. The later Penina observations (sol 1986 and 2024) show a marked decrease in 100–300 μm grains and aggregated particles, leaving a lag of larger, subangular sand particles (Figure 23). Grain size distributions measured at the Penina target confirm that the mean grain size increases between sols 1936 and 2024 [*Siebach et al.*, 2010; *Arvidson et al.*, 2010]. At Sackrider, the initial MI observation (sol 1922) is dominated by 100–300 μm grains and aggregates which crush easily under the 1N force of the MB, creating a high-fidelity cast of the smooth MB plate surface and a raised circle of uncompressed material in the center of the sol 1925 observation (Figures 24a–24b). By the sol 1982 Sackrider observation (Figure 24c), the soil is dominated by a spatially heterogeneous distribution of >300 μm fine to medium sand particles.

5. Discussion

[52] At the Tyrone soil exposure, the most significant changes observed in Pancam spectra were an increase in the 535 nm band depth over 152 sols (Figure 4b), and an increase in the red to blue (753 nm to 432 nm) ratio during the first 74 sols with no statistically significant change thereafter (Figure 4d). The percent change maps for these parameters (Figures 5a–5b) agree with the image-based observations. The 535 nm band depth percent change map (Figure 5a) shows that this parameter systematically increased between sols 864 and 1005 by ~120% for both the white and yellow soil hues, which is the largest change observed for any material in the image. An increase in 535 nm band depth is consistent with dehydration based on our laboratory experiments (Figure 18), but is also consistent with contami-

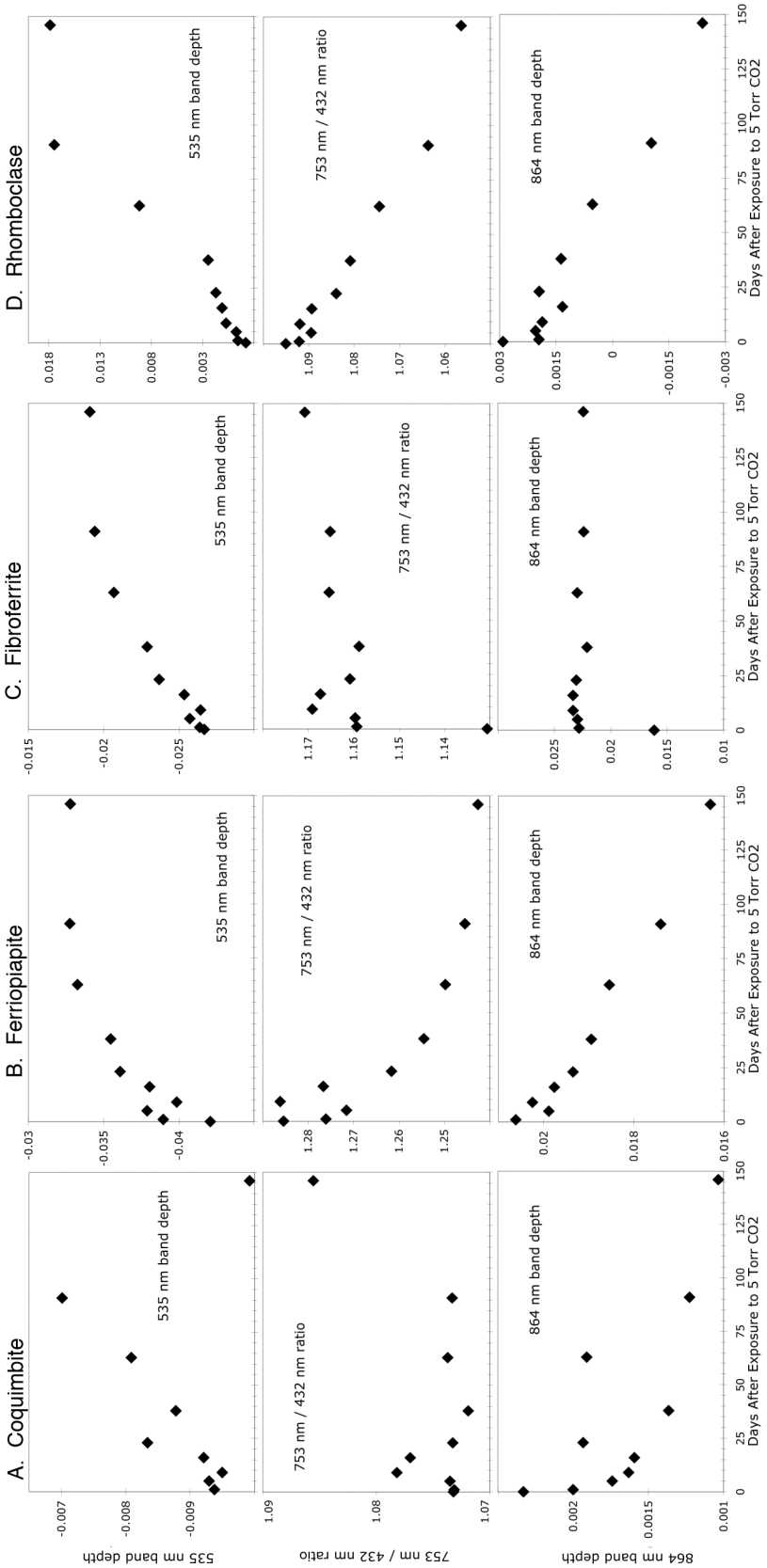

Figure 18. Spectral parameters (535 nm band depth, 753 nm/432 nm slope, and 864 nm band depth) measured from laboratory spectra of ferric sulfate minerals exposed to Martian surface conditions (P = 5 Torr CO_2; T = 20°C) over the first 150 days of the experiment: (a) coquimbite, (b) ferricopiapite, (c) fibroferrite, and (d) rhomboclase. See text for experimental procedure.

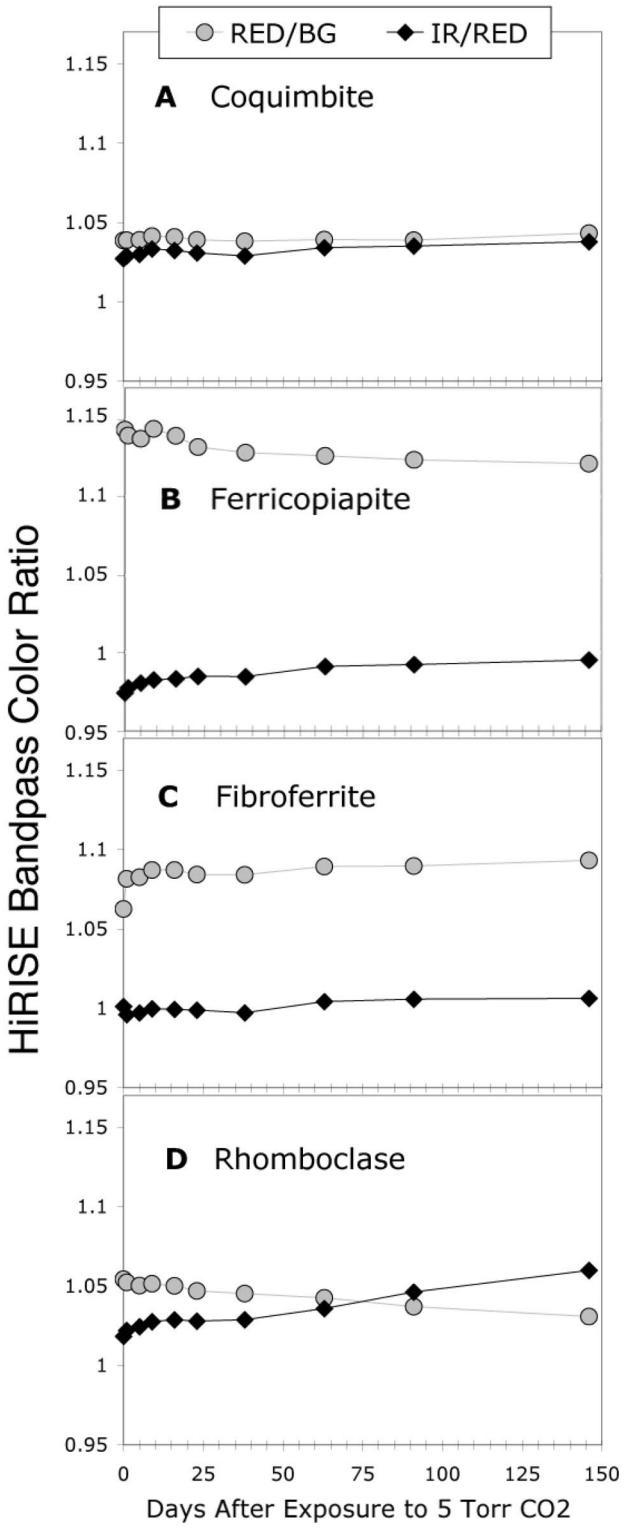

Figure 19. Color ratios (RED/BG and IR/RED) of HiRISE band passes (BG = 502 ± 157 nm; RED = 686 ± 267 nm; IR = 878 ± 143 nm) measured from laboratory spectra of ferric sulfate minerals exposed to Martian surface conditions (P = 5 Torr CO_2; T = 20°C) over the first 150 days of the experiment: (a) coquimbite, (b) ferricopiapite, (c) fibroferrite, and (d) rhomboclase. See text for experimental procedure.

nation by air fall dust and/or aeolian mixing with surrounding dusty soils, which have relatively deep 535 nm features in Pancam spectra (e.g., Figures 3 and 4a). Because the 535 nm band depth is also observed to increase for dark, basaltic float rocks in the scene (Figure 5a), the effect of air fall dust may explain the observations. Therefore, on its own, an increase in 535 nm band depth is not a unique or definitive indicator of mineralogic change.

[53] The 753 nm to 432 nm ratio percent change map (Figure 5b) indicates that this parameter increases at the Tyrone white soil with respect to other materials between sols 864 and 1005. However, the average magnitude of this change is only 4%, which is smaller than the typical pixel-to-pixel variations within the white soil deposit (±7%). In the image-based analysis (Figure 4d), we observe that the only statistically significant change to the red to blue ratio occurred between sols 790 and 864. An increase in this ratio is inconsistent with the spectral changes associated with the dehydration of ferric sulfates (Figure 18); it is consistent, however, with dust contamination over 74 sols, which would "redden" the soil color. Thus, the effects of air fall dust contamination alone could explain the increases in the 535 nm band depth and red to blue ratio observed at the Tyrone soils.

[54] The trends in Spirit's solar array energy can be used to infer dust deposition and wind activity over the period of observation [e.g., *Landis et al.*, 2004]. The power from the solar panels varies with season and atmospheric optical depth (tau in Table 2), degrades slowly from continual air fall dust accumulation, and increases sharply following strong wind events that remove dust from the solar panels. Over sols 790 to 1062 (Figure 25), no large solar panel cleaning events occurred during the Tyrone imaging campaign. The gradual decrease in solar array energy over the Tyrone imaging campaign (from 357 to 288 W-hrs), even after the winter solstice on sol 923 (when the solar insolation begins to increase), indicates a period of low winds and gradual dust deposition during Spirit's winter at Low Ridge. This decrease is consistent with the minor spectral variations observed at the Tyrone soil exposure reflecting contamination by air fall dust, and not aeolian mixing or a mineralogic change.

[55] Our results cannot confirm the initial Pancam-based study by *Wang et al.* [2008], who reported a decrease in the 432 to 753 spectral slope of the Tyrone yellow soil hue between sols 864 and 1062, with the largest change occurring between sols 922 and 959. Those spectral changes were interpreted as evidence for a mineralogic phase change of the exposed yellow soil. While we do observe a minor decrease in the 753 to 432 nm ratio between sols 922 and 959 (Figure 4d), we show above that this difference is well within the statistical noise, as are all of the other variations of this parameter between sols 864 and 1062 for the yellow and white soils.

[56] *Wang et al.* [2008] based their results on a visual, qualitative analysis of 432 nm versus 753 nm histograms from each observation, in which the data cloud containing pixels from the yellow soil was observed to change relative to the data cloud containing pixels from the white soil [*Wang et al.*, 2008, Figure 27]. However, small, qualitative variations in the shapes and positions of data clouds such as two-dimensional histograms might not accurately represent

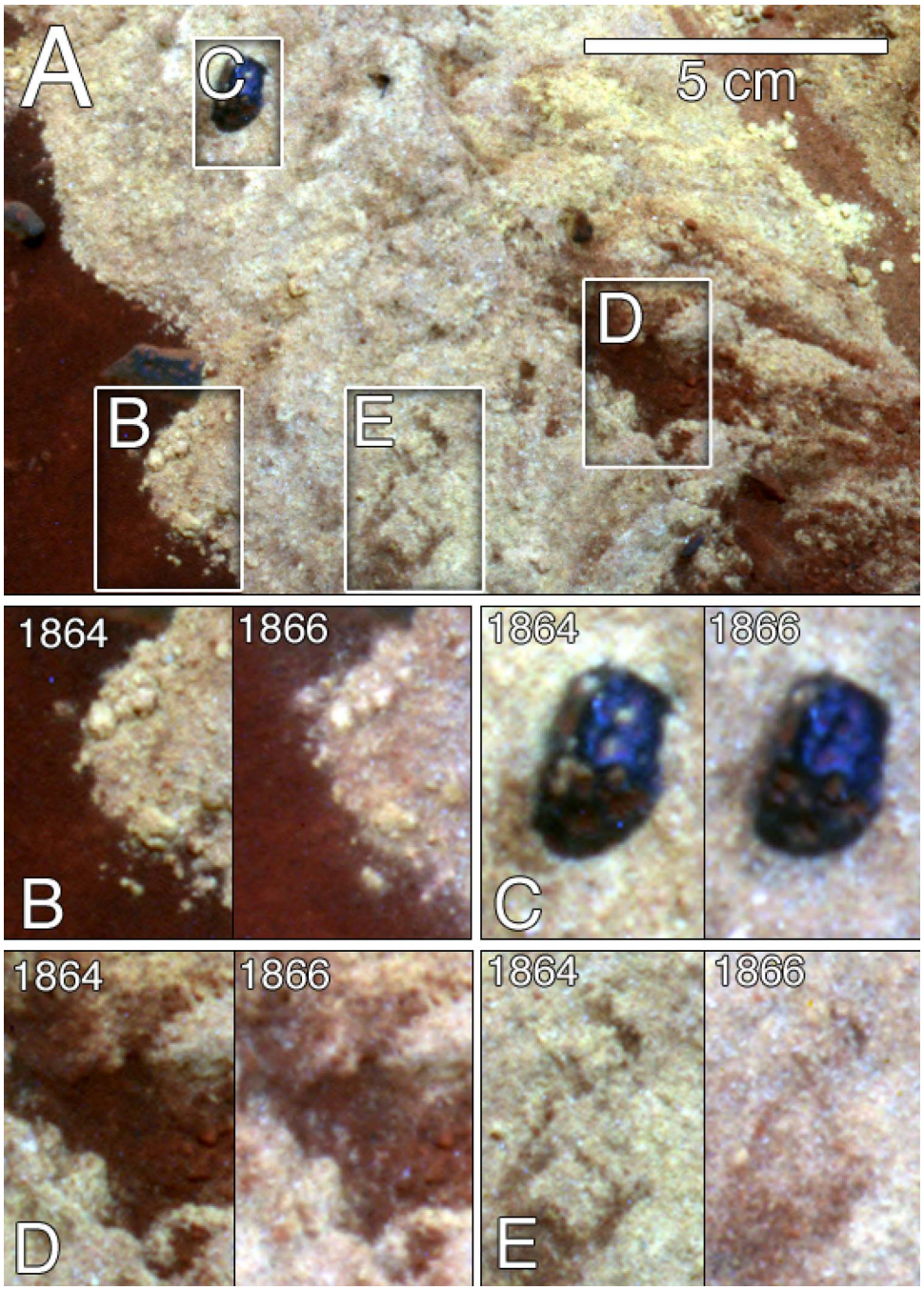

Figure 20. Examples of textural changes at the Kit Carson soil exposure between sols 1864 and 1866. (a) False color image (blue, 432 nm; green, 535 nm; red, 753 nm) from sol 1864 (P2562) showing the locations of Figures 20b–20e. (b) Partial disintegration of soil clod and movement of fines, (c) removal of fines from basaltic pebble, (d) appearance of light-toned material upon dark soil, and (e) disintegration of soil clods and homogenization of texture. Note that the two Pancam images are not shown at the same color stretch and should only be used for textural comparisons, not color comparisons. Location of Figure 20a is indicated in Figure 9a.

the actual level of statistical variations within an individual image, or between sets of subsequent images. For example, visual methods for detecting changes in the centroid of a histogram data cloud are highly sensitive to how histogram frequency values are displayed on a plot. If all values in the histogram are displayed in the same or similar color or gray scale, for example, then outliers of relatively insignificant numbers of pixels could be perceived as having much greater statistical weight than they should actually have. A more rigorous weighting of each histogram bin is critical in order to accurately assess variations in a data cloud.

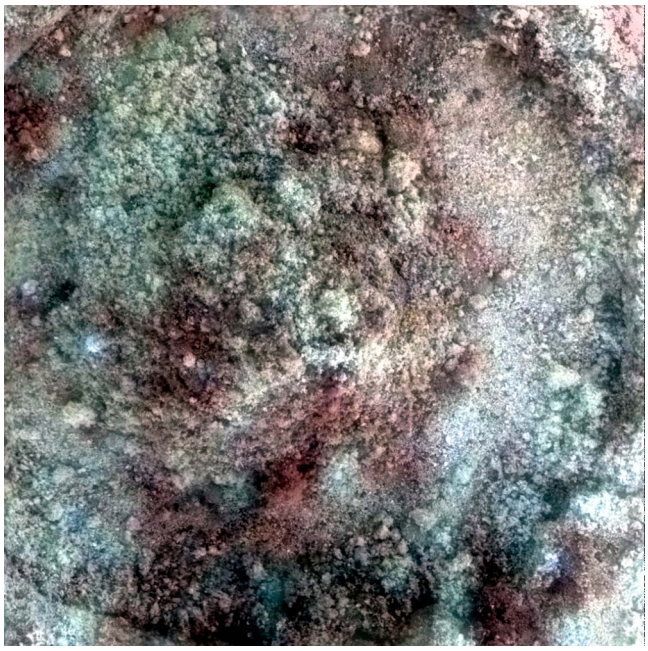

Figure 21. Merge of calibrated MI image 2M291757408, acquired on sol 1863 when target was fully shadowed, and Pancam L257 enhanced color image, acquired on sol 1866 of the John Wesley Powell target within the Kit Carson soil exposure. Location is shown in Figure 9c. Field of view is ~3 cm.

[57] At the Gertrude Weise exposure, we observed no statistically significant spectral changes, implying that Pancam detected no dehydration of the silica-rich material. The solar array energy data (Figure 25) indicates that no strong wind events or significant dust deposition occurred during the 50 sol period of observation, supporting the contention that aeolian mixing did not occur between sols 1158 and 1198.

[58] The increase in 864 nm band depth of Kit Carson white and yellow soils is the most statistically significant spectral change observed by Pancam at any soil exposure (Figure 11). However, this increase is inconsistent with expected spectral changes from the dehydration of the ferric sulfates that we studied (section 3.3), and is also inconsistent with dust deposition or aeolian mixing because all other scene materials have shallower 864 nm band depths than the bright soil (Figure 11). While an increase of this band depth could be consistent with the rehydration of a ferric sulfate mineral (in the case where pH_2O is greater at the Martian surface than in the near subsurface), we consider this an unlikely scenario because the magnitude of the observed change is so large – the 200% increase in 864 nm band depth observed over two sols is greater than the largest change observed in our laboratory experiments of ferric sulfates equilibrating to Martian conditions from Earth conditions over 150 days (130% decrease in 864 nm band depth for coquimbite). Furthermore, no other spectral changes that would be expected to accompany rehydration have been observed, such as a decrease in 535 nm band depth or an increase in 753 nm to 432 nm ratio (from the reverse of trends shown in Figure 18).

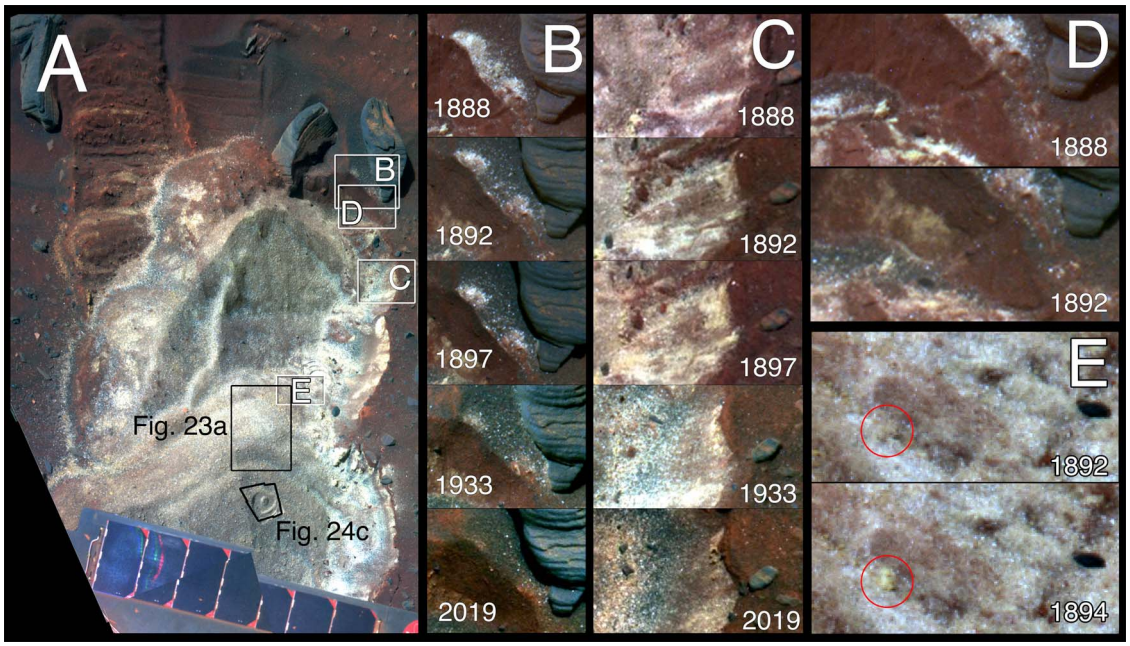

Figure 22. Examples of textural changes at the Ulysses soil exposure between sols 1888 and 2019. (a) False color image (blue, 432 nm; green, 535 nm; red, 753 nm) from sol 1933 (P2382) showing the locations of Figures 22b–22e, as well as Figure 23a and Figure 24a. The wheel track in the top left is ~16 cm wide. (b) Disappearance of fine white material, (c) dispersal and removal of light material along the cliff at the eastern edge of the exposure, (d) appearance of bright material in cliff at the northern edge of the exposure, and (e) appearance of a bright soil clod (marked by the red circle) within the exposure.

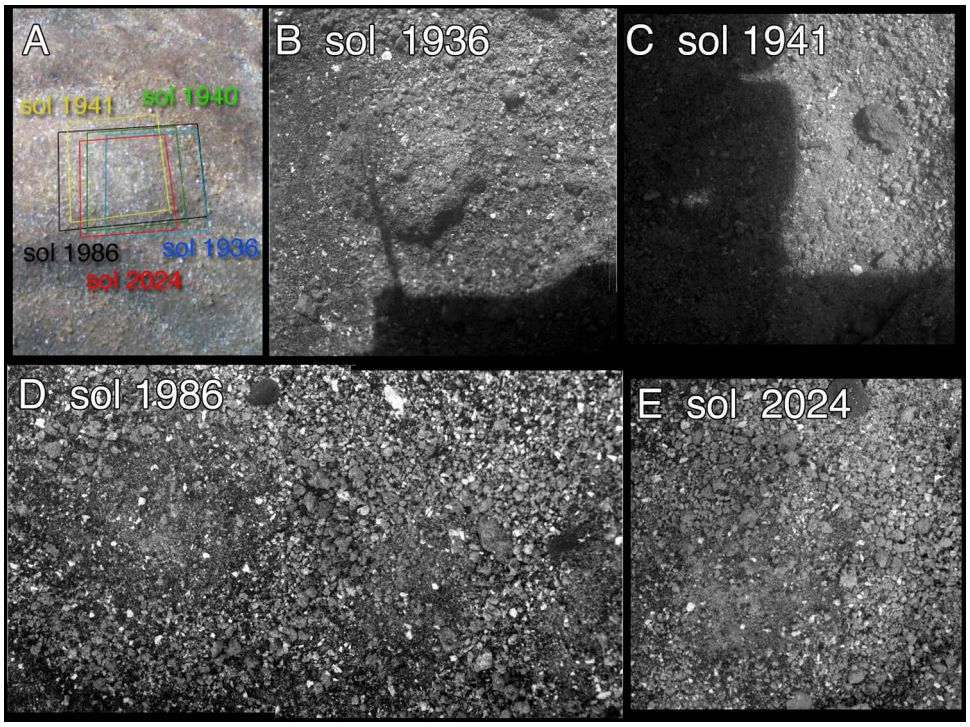

Figure 23. Observations of Penina. Each MI observation is ~3 cm high. (a) Pancam image with footprints of MI observations. (b) Merge of 6 MI images acquired on sol 1936 when the target was partly shadowed. (c) Merge of 5 MI images acquired on sol 1941 when the target was partly shadowed. (d) Mosaic of 2 MI images acquired on sol 1986 when the target was fully shadowed. (e) MI image 2M306051999 acquired on sol 2024 when target was fully shadowed. Location of Figure 23a is shown in Figure 22a.

[59] The observed 864 nm band depth increase at Kit Carson could instead represent an instrumental or observational effect rather than a physical change, because (1) the magnitude of the observed change is so large; (2) it is the only significant spectral change observed; (3) an increase in 864 band depth is inconsistent with dust deposition, aeolian sorting or mineral dehydration; and (4) the spectra extracted from the two Pancam observations were variably affected by the dust contamination effects described in section 2.1.4 (because the ROIs were extracted from different regions of the FOV; Figure 9). We performed a first-order correction for dust contamination by considering the spectral parameters as ratios of the bright soil targets to undisturbed soils imaged in similar regions of the FOV, rather than as absolute values (see section 2.1.4); however, our assumption that the contamination affects similar regions of the FOV by the same scale factor is incorrect. Further work is needed to understand the effects of dust contamination on the Pancam optics late in Spirit's mission.

[60] No changes were observed in HiRISE color data over a 32 sol period that would indicate a mineralogic change, dust deposition, or aeolian sorting event; all measurements of relative color ratio for the Kit Carson, Gertrude Weise and Tyrone soils were <5% and smaller than the estimated errors (Figure 16). For comparison, the relative I/F decrease in the BG filter observed for exposed ice by *Byrne et al.* [2009] ranged from 20% to 60%. Based on convolutions of our laboratory spectra to HiRISE band passes (Figure 19), we would not expect the dehydration of ferric sulfate minerals following exposure to the Martian surface to be detectable above the uncertainties in HiRISE observations. However, we would expect extensive dust deposition and/or aeolian mixing to be detectable as an increase in the RED/BG ratio. The nondetection of changes is consistent with the solar array data (Figure 25), which indicate no major dust deposition between sols 1935 and 1967. We note that later changes to the Gusev soils have been observed by HiRISE, as all bright soil exposures are no longer visible in the sol 2177 RED observation (Figure 15c).

[61] The nondetection of mineralogic changes from Pancam and HiRISE data may indicate that highly hydrated ferric sulfates are not actually present in the bright soil exposures. None of Spirit's instruments have unambiguously identified the minerals used in our lab study at the Gusev bright soil exposures, and the Pancam spectral deconvolution studies did not include anhydrous ferric-bearing sulfates in their libraries (with the exception of yavapaiite) [*Johnson et al.*, 2007; *Lane et al.*, 2008; *Parente et al.*, 2009], so it is a possibility that the sulfate-rich soils consist largely of anhydrous phases. The nondetection could also indicate that any hydrated mineral components of the Gusev bright soil exposures were in equilibrium with Martian surface conditions prior to exposure, or that the spectral changes accompanying mineral dehydration were below the instrument detection limits.

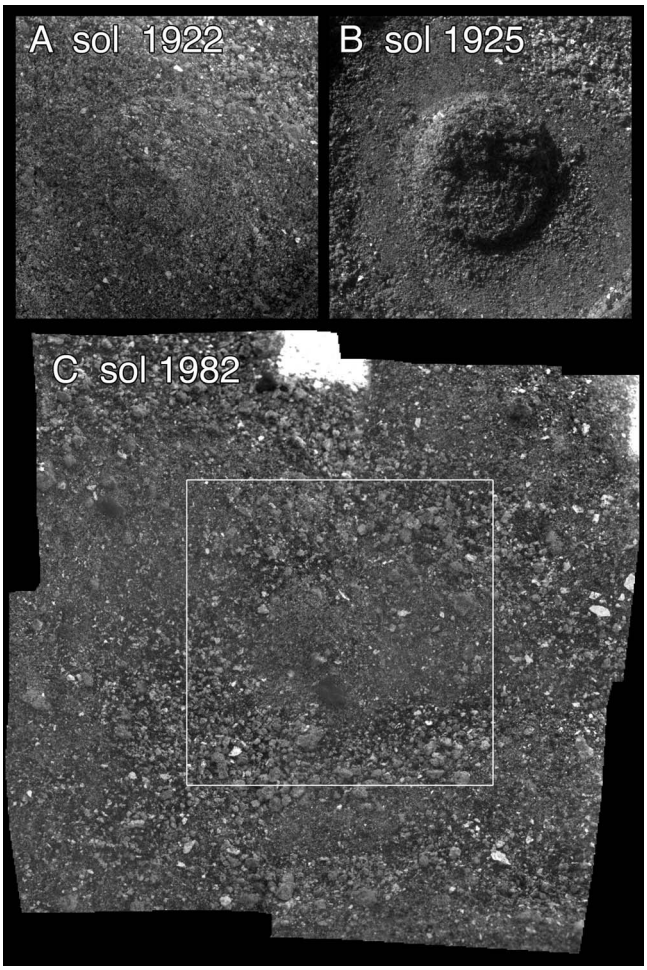

Figure 24. Microscopic Imager (MI) observations of Sackrider. (a) Merge of 5 MI images acquired on sol 1922 when target was fully shadowed. Image is ~3 cm across. (b) Merge of 5 MI images acquired on sol 1925 when target was illuminated from the top left. Image is ~3 cm across. (c) Mosaic of 4 MI images acquired on sol 1982 when target was mostly shadowed. White box in indicates location of Figures 24a and 24b; mosaic is ~5 cm across. Location of Figure 24c is shown in Figure 22a.

[62] Alternately, the dehydration of the bright soils may be inhibited by slow reaction kinetics at low temperatures, as has been proposed for the Mg-sulfates of Candor Chasma by *Roach et al.* [2009]. Using two years of Compact Reconnaissance Imaging Spectrometer (CRISM) and Observatoire pour la Minéralogie, l'Eau, les Glaces et l'Activité (OMEGA) observations, *Roach et al.* [2009] found no spectral changes indicative of changes in hydration state of the monohydrated or polyhydrated sulfates, although only one hydration state should be stable at a given time. The authors suggest that the thermodynamically predicted conversion between Mg-sulfate phases is limited by reaction kinetics at low Martian surface temperatures, which may be the case for ferric sulfate phases at Gusev crater as well (the average surface temperature at Gusev crater is significantly lower than the +20°C used in our laboratory experiments).

[63] The observed textural changes at Kit Carson directly reveal movement of fine particles by wind. Wind is the only explanation for the removal of material from depressions on the small cobble, for example, and for the appearance of bright material on dark portions of the wheel trench (Figures 20c–20d). Because there was no significant change in dust factor between sols 1864 and 1866 (Figure 25), the observed changes must have been caused by winds too small (or too close to the ground) to remove a significant amount of dust from the rover deck. The only textural change that would be consistent with dehydration is the dispersal of the soil clod in Figure 20b, which could occur upon desiccation. However, a weakly bound soil aggregate, such as those seen in the MI image in Figure 21, could also disperse if impacted by a particle traveling on a wind-driven trajectory (although no lineations or streaks of bright material, as would be expected from this scenario, are observed). Some spectral variations observed at Kit Carson have resulted from these textural changes, such as the increase in reflectance of dark disturbed soil from contamination by windblown, fine-grained, bright soil, as illustrated in Figure 20d.

[64] The many spectral and textural changes observed at Ulysses are also related. The changes in the Pancam spectral parameters show that the white and yellow soils grew less distinct from the dark disturbed materials over time (Figure 14), and the spectra of white and yellow hues converged (Figure 13). This convergence is illustrated well in DCS images, where the two distinct hues seen in the sol 1888 observation are no longer distinguishable in the sol 1982 observation (Figure 12). These spectral and color changes are consistent with aeolian mixing of bright materials with basaltic soils in the trench. A large wind event(s) between the sol 1897 and sol 1933 observations, illustrated as an increase in solar array energy in Figure 25, likely mobilized and removed at least some of the finest grains. Monitoring of the rover deck with Pancam images of the calibration target also showed significant cleaning after sol 1896 until sol 2003, when dust was again deposited on the deck. The Sackrider and Penina MI observations confirm the removal of fine, bright material, leaving behind the coarsest size fraction of the bright materials mixed with basaltic sand-sized grains.

[65] We interpret some textural changes to result from the slumping of material at the angle of repose. Fine-grained bright material is seen to have moved downslope from the ridge at the west of the Kit Carson exposure (Figure 20b, top). The bright material that "appears" along the Ulysses trench wall between sols 1888 and 1982 (Figure 22d) has likely been exposed from underneath dark material along the wall that has slumped into the trench. This gravity-driven mobility exemplifies the unconsolidated nature of both the dark and bright exposed materials.

[66] Textural modifications occur outside the bright deposits as well, such as softening of the imprints created by the wheel cleats in dusty surface soil at Ulysses (Figure 22a, top). We do not observe any wind-related changes to surfaces that have not been disturbed by wheels, however, because induration of the Martian regolith in this area has apparently immobilized surface grains [e.g., *Sullivan et al.*, 2008]. As seen in the Ulysses eastern cliff (Figure 22c), the topmost soil layer consists of a series of ~1 cm crust-like layers of cohesive, perhaps cemented grains.

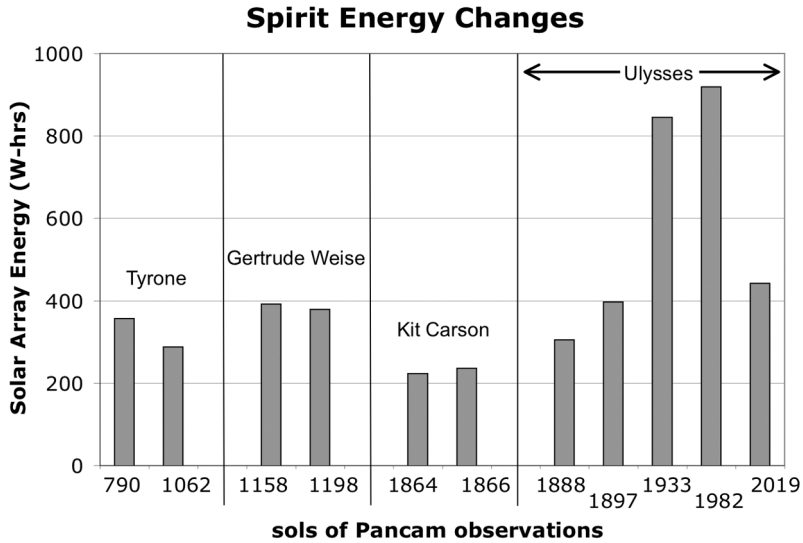

Figure 25. Spirit solar array energy for the sols of imaging campaigns considered in this study: Tyrone (sols 790–1062), Gertrude Weise (sols 1158–1198), Kit Carson (sols 1864–1866), and Ulysses (sols 1888–2019). The increase in array energy between sols 1897 and 1933 indicates a strong wind event that cleaned dust from the rover deck; decreases in array energy indicate dust deposition on the solar panels.

[67] Our observations of wind-driven particle movement are consistent with previous studies of particle mobility at Gusev crater. The majority of grain movement has been shown to occur in brief episodes of entrainment and saltation during strong wind events, and sand grains (~100 μm) have been noted to appear on Spirit's solar panel deck 0.66 m above the ground following periods of high winds [*Greeley et al.*, 2006]. *Sullivan et al.* [2008] showed that low density, sand-sized (several hundred μm) aggregates of air fall dust are more easily mobilized than solid particles of the same size; in the MI observations at Ulysses, we observe that the same is true of porous bright soil aggregates, which are more easily mobilized than soil grains of the same size (the solid

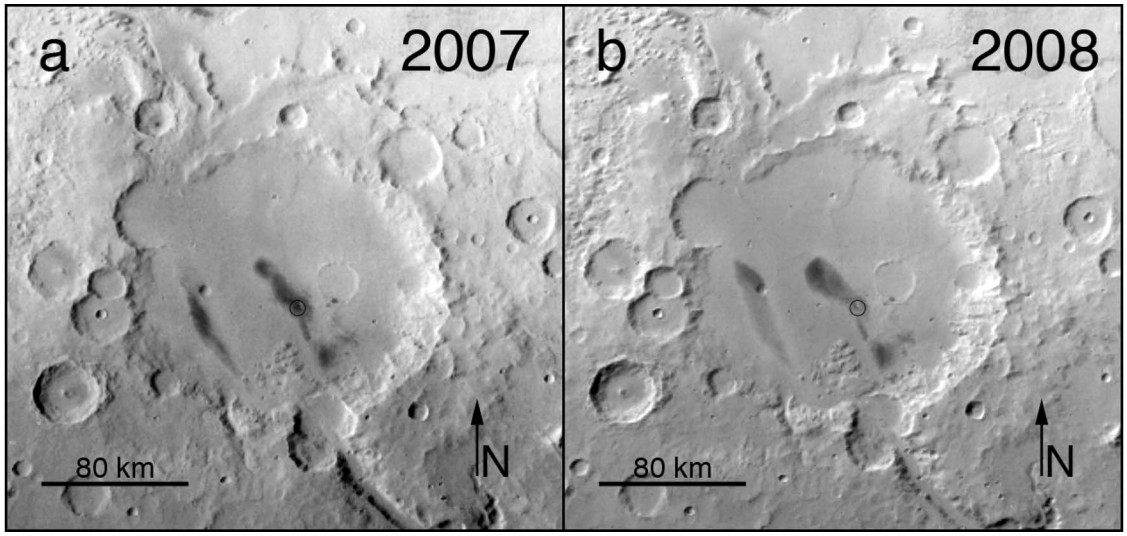

Figure 26. Mosaics of Gusev crater from the Mars Reconnaissance Orbiter Mars Color Imager (MARCI) band 5 (718 ± 50 nm). The mosaics were generated by map-projecting all MARCI images of Gusev crater in (a) 2007 (sols 1064–1419) and (b) 2008 (sols 1420–1775) for which spacecraft pointing and ephemeris (SPICE) information was available. To minimize the effects of atmospheric dust, each pixel in the mosaic was assigned the lowest albedo value for that location from the list of overlapping map-projected images. The black circles indicate the location of the Columbia Hills and the Spirit rover. The changes to the low-albedo wind streaks exemplify the large-scale wind activity and dust movement that has occurred over the period discussed in this work.

>300 μm grains remain in the trench as a lag deposit; Figures 23–24).

[68] Spirit has observed hundreds of dust devils during its mission [*Waller et al.*, 2009], and dust devil tracks in Gusev crater have been observed from orbit [*Greeley et al.*, 2003]. The strong wind events recorded in Spirit's solar array energy and seen in Pancam and MI data also caused dramatic changes in the low-albedo wind streaks in Gusev crater. This is apparent in repeated observations of the region by the Mars Reconnaissance Orbiter Mars Color Imager (MARCI) [*Bell et al.*, 2009] (Figure 26). The observed dust devil and wind streak activity indicates that Gusev crater was an active region of dust removal and deposition during the time period discussed in this work.

6. Conclusions

[69] We have compared repeated multispectral observations of the Tyrone, Gertrude Weise, Kit Carson and Ulysses bright soils to test the hypothesis that the ferric sulfate and silica-rich materials undergo mineralogic changes upon exposure. In Pancam and HiRISE data, we observe no statistically significant spectral changes that are uniquely diagnostic of dehydration and/or mineralogic phase changes. In Pancam and MI observations of Kit Carson and Ulysses, we have also observed no textural changes that are consistent with the desiccation of a hydrated mineral. We conclude that there is no unique or statistically reliable evidence for mineralogic changes following the exposure of the Gusev bright soils. Our nondetections do not prove that no mineralogic changes occurred in the soils examined in this study. However, if any mineralogic changes did occur, they were below the detection threshold of the Pancam instrument.

[70] We have observed several spectral and textural changes that are consistent with air fall dust deposition and wind-driven particle movement. The Tyrone bright soil spectra converge toward the spectral characteristics of Martian dust over the 272 sols of observation (e.g., the 753 nm to 432 nm ratio and the 535 nm band depth increase), consistent with contamination by air fall dust. The hue separations at Ulysses become less distinct over the 131 sols of observation, which we interpret as evidence of aeolian mixing within the trench. At Kit Carson and Ulysses, we observe significant textural changes, including slumping within the wheel trench, winnowing of fines, movement of soil aggregates, and dispersal of soil aggregates. Our observations are consistent with previous studies that have shown that strong wind events mobilize the <300 μm soil fraction and can entrain larger, porous soil aggregates [e.g., *Greeley et al.*, 2006; *Sullivan et al.*, 2008]. Thus, to varying degrees, all of the observed changes to the spectra and textures of the bright Gusev soil exposures can be attributed to air fall dust deposition and aeolian sorting.

[71] **Acknowledgments.** We gratefully acknowledge our colleagues on the Mars Exploration Rover and MRO HiRISE teams at the Jet Propulsion Laboratory, Cornell University, USGS/Flagstaff, University of Arizona, and other partner institutions for enabling us to study the surface of Mars from microscopic to orbital scales. We thank Jonathan Joseph for his help in the calibration of Pancam images, Stan Mertzman for the compositional analysis of the ferric sulfate samples, Richard Morris for insightful suggestions that strengthened this work, Anya Portyankina and M. Vincendon for providing dust-corrected HiRISE images, and Alicia Vaughan and Jennifer Herman for their help with the presentation of Spirit's array energy. Leah Roach and an anonymous reviewer provided thoughtful comments that improved the quality of this work. This work is supported by grants and contracts from the NASA Mars Exploration Program (JPL) and the Mars Data Analysis Program (Cornell). M.S.R. was supported by a National Science Foundation Graduate Research Fellowship. E.A.C. and his lab facility are supported by grants from CSA, NSERC, CFI, MRIF, and the University of Winnipeg. J.J.W. thanks the NSF and the Fannie and John Hertz Foundation for support.

References

Arvidson, R. E., et al. (2010), Spirit Mars Rover Mission: Overview and selected results from the northern Home Plate Winter Haven to the side of Scamander crater, *J. Geophys. Res.*, *115*, E00F03, doi:10.1029/2010JE003633.

Bell, J. F., III, et al. (2003), The Mars Exploration Rover Athena Panoramic Camera (Pancam) investigation, *J. Geophys. Res.*, *108*(E12), 8063, doi:10.1029/2003JE002070.

Bell, J. F., III, J. Joseph, J. N. Sohl-Dickstein, H. M. Arneson, M. J. Johnson, M. T. Lemmon, and D. Savransky (2006), In-flight calibration and performance of the Mars Exploration Rover Panoramic Camera (Pancam) Instruments, *J. Geophys. Res.*, *111*, E02S03, doi:10.1029/2005JE002444.

Bell, J. F., III, et al. (2009), Mars Reconnaissance Orbiter Mars Color Imager (MARCI): Instrument description, calibration, and performance (2009), *J. Geophys. Res.*, *114*, E08S92, doi:10.1029/2008JE003315.

Byrne, S., et al. (2009), Distribution of mid-latitude ground ice on Mars from new impact craters, *Science*, *325*, 1674–1676, doi:10.1126/science.1175307.

Chipera, S., D. Vaniman, and D. L. Bish (2007), The effect of temperature and water on ferric-sulfates, *Lunar Planet. Sci.*, *XXXVIII*, Abstract 1409.

Cloutis, E. A., M. A. Craig, R. V. Kruzelecky, W. R. Jamroz, A. Scott, F. C. Hawthorne, and S. A. Mertzman (2008), Spectral reflectance properties of minerals exposed to simulated Mars surface conditions, *Icarus*, *195*, 140–168, doi:10.1016/j.icarus.2007.10.028.

Craig, M. A., E. A. Cloutis, and T. Mueller (2001), ME and Mini-ME: Two Mars environmental simulation chambers for reflectance spectroscopy, *Lunar Planet. Sci.*, *XXXII*, Abstract 1368.

Delamere, W. A., et al. (2010), Color imaging of Mars by the High Resolution Imaging Science Experiment (HiRISE), *Icarus*, *205*, 38–52, doi:10.1016/j.icarus.2009.03.012.

Farrand, W. H., J. F. Bell III, J. R. Johnson, R. E. Arvidson, L. S. Crumpler, J. A. Hurowitz, and C. Schröder (2008), Rock spectral classes observed by the Spirit Rover's Pancam on the Gusev crater plains and in the Columbia Hills, *J. Geophys. Res.*, *113*, E12S38, doi:10.1029/2008JE003237.

Freeman, J., A. Wang, and Z. Ling (2009), Ferric sulfates on Mars: Mission observations and laboratory investigations, *Lunar Planet. Sci.*, *XL*, Abstract 2284.

Gellert, R., et al. (2006), Alpha Particle X-ray Spectrometer (APXS): Results from Gusev crater and calibration report, *J. Geophys. Res.*, *111*, E02S05, doi:10.1029/2005JE002555.

Gillespie, A., A. Kahle, and R. Walker (1986), Color enhancement of highly correlated images. I. Decorrelation and HSI contrast stretches, *Remote Sens. Environ.*, *20*(3), 209–235.

Greeley, R., R. O. Kuzmin, and S. C. R. Rafkin (2003) Wind-related features in Gusev crater, Mars, *J. Geophys. Res.*, *108*(E12), 8077, doi:10.1029/2002JE002006.

Greeley, R., et al. (2006), Gusev crater: Wind-related features and processes observed by the Mars Exploration Rover Spirit, *J. Geophys. Res.*, *111*, E02S09, doi:10.1029/2005JE002491.

Hapke, B. (1993), *Theory of Reflectance and Emittance Spectroscopy*, Cambridge Univ. Press, Cambridge, UK, doi:10.1017/CBO9780511524998.

Herkenhoff, K. E., et al. (2003), Athena Microscopic Imager investigation. *J. Geophys. Res.*, *108*(E12), 8065, doi:10.1029/2003JE002076.

Herkenhoff, K. E., et al. (2006), Overview of the Microscopic Imager investigation during Spirit's first 450 sols in Gusev crater, *J. Geophys. Res.*, *111*, E02S04, doi:10.1029/2005JE002574.

Johnson, J. R., et al. (2006), Spectrophotometric properties of materials observed by Pancam on the Mars Exploration Rovers: 1. Spirit, *J. Geophys. Res.*, *111*, E02S14, doi:10.1029/2005JE002494.

Johnson, J. R., J. F. Bell III, E. Cloutis, M. Staid, W. H. Farrand, T. McCoy, M. Rice, A. Wang, and A. Yen (2007), Mineralogic constraints on sulfur-rich soils from Pancam spectra at Gusev crater, Mars, *Geophys. Res. Lett.*, *34*, L13202, doi:10.1029/2007GL029894.

Kinch, K. J., J. Sohl-Dickstein, J. F. Bell III, J. R. Johnson, W. Goetz, and G. A. Landis (2007), Dust deposition on the Mars Exploration Rover Panoramic Camera (Pancam) calibration targets, *J. Geophys. Res.*, *112*, E06S03, doi:10.1029/2006JE002807.

Landis, G. A., T. W. Kerslake, P. Jenkins, and D. Scheiman (2004), Mars solar power, paper presented at 2nd International Energy Conversion Engineering Conference, Am. Inst. of Aeronaut. and Astronaut., Providence.

Lane, M., J. Bishop, M. Darby Dyar, P. King, M. Parente, and B. Hyde (2008), Mineralogy of the Paso Robles soils on Mars, *Am. Mineral.*, *93*, 728–739, doi:10.2138/am.2008.2757.

Lemmon, M. T., et al. (2004), Atmospheric imaging results from the Mars Exploration Rovers: Spirit and Opportunity, *Science*, *306*, 1753–1756, doi:10.1126/science.1104474.

Maki, J. N., et al. (2003), The Mars Exploration Rover Engineering Cameras, *J. Geophys. Res.*, *108*(E12), 8071, doi:10.1029/2003JE002077.

McEwen, A. S., et al. (2007), Mars Reconnaissance Orbiter's High Resolution Imaging Science Experiment (HiRISE), *J. Geophys. Res.*, *112*, E05S02, doi:10.1029/2005JE002605.

McEwen, A. S., et al. (2010), The High Resolution Imaging Science Experiment (HiRISE) during MRO's Primary Science Phase (PSP), *Icarus*, *205*, 2–37, doi:10.1016/j.icarus.2009.04.023.

Mertzman, S. A. (2000), K-Ar results from the southern Oregon-northern California cascade range, *Oregon Geol.*, *62*, 99–122.

Ming, D. W., et al. (2006), Geochemical and mineralogical indicators for aqueous processes in the Columbia Hills of Gusev crater, Mars, *J. Geophys. Res.*, *111*, E02S12, doi:10.1029/2005JE002560.

Ming, D. W., et al. (2008), Geochemical properties of rocks and soils in Gusev crater, Mars: Results of the Alpha Particle X-ray Spectrometer from Cumberland Ridge to Home Plate, *J. Geophys. Res.*, *113*, E12S39, doi:10.1029/2008JE003195.

Morris, R. V., and G. Klingelhöfer (2008), Iron mineralogy and aqueous alteration on Mars from the MER Mössbauer spectrometer, in *The Martian Surface - Composition, Mineralogy, and Physical Properties*, edited by J. F. Bell, III, pp. 339–365, Cambridge Univ. Press, Cambridge, UK, doi:10.1017/CBO9780511536076.016.

Morris, R. V., et al. (2006), Mössbauer mineralogy of rock, soil, and dust at Gusev crater, Mars: Spirit's journey through weakly altered olivine basalt on the plains and pervasively altered basalt in the Columbia Hills, *J. Geophys. Res.*, *111*, E02S13, doi:10.1029/2005JE002584.

Morris, R. V., et al. (2008), Iron mineralogy and aqueous alteration from Husband Hill through Home Plate at Gusev crater, Mars: Results from the Mössbauer instrument on the Spirit Mars Exploration Rover, *J. Geophys. Res.*, *113*, E12S42, doi:10.1029/2008JE003201.

Parente, M., J. L. Bishop, and J. F. Bell III (2009), Spectral unmixing for mineral identification in pancam images of soils in Gusev crater, Mars, *Icarus*, *203*, 421–436, doi:10.1016/j.icarus.2009.04.029.

Portyankina, G., M. Vincendon, N. Thomas, and K.-M. Aye (2010), Recovery of surface reflectance from atmospheric aerosol contribution: Application to HiRISE images, *Lunar Planet. Sci.*, *XLI*, Abstract 1582.

Reid, R. J., P. Rueffer, F. Gliem, J. R. Johnson, J. N. Maki, K. E. Herkenhoff, and R. B. Singer (1999), Imager for Mars Pathfinder (IMP) image calibration, *J. Geophys. Res.*, *104*, 8907–8925, doi:10.1029/1998JE900011.

Rice, M. S., J. F. Bell III, E. A. Cloutis, A. Wang, S. Ruff, M. A. Craig, D. T. Bailey, J. R. Johnson, P. A. de Souza Jr., and W. H. Farrand (2010a), Silica-rich deposits and hydrated minerals at Gusev crater, Mars: Vis-NIR spectral characterization and regional mapping, *Icarus*, *205*, 375–395, doi:10.1016/j.icarus.2009.03.035.

Rice, M. S., E. Cloutis, and J. Crowley (2010b), Spectral reflectance changes accompanying long-duration exposure of silica sinter and Fe-sulfates to simulated Mars surface conditions, *Lunar Planet. Sci.*, *XLI*, Abstract 2576.

Roach, L. H., J. F. Mustard, S. L. Murchie, J.-P. Bibring, F. Forget, K. W. Lewis, O. Aharonson, M. Vincedon, and J. L. Bishop (2009), Testing evidence of recent hydration state change in sulfates on Mars, *J. Geophys. Res.*, *114*, E00D02, doi:10.1029/2008JE003245.

Siebach, K., R. E. Arvidson, N. Cabrol, and the Athena Science Team (2010), Recent Spirit Results: Microscopic Imager analysis of particle properties in Scamander crater, west of Home Plate, *Lunar Planet. Sci.*, *XLI*, Abstract 2548.

Sohl-Dickstein, J., J. R. Johnson, W. M. Grundy, E. Guinness, T. Graff, M. K. Shepard, R. E. Arvidson, J. F. Bell III, P. Christensen, and R. Morris (2005), Modeling visible/near-infrared photometric properties of dustfall on a known substrate, *Lunar Planet. Sci.*, *XXXVI*, Abstract 2235.

Squyres, S. W., et al. (2008), Discovery of silica-rich deposits on Mars by the Spirit Rover, *Science*, *320*, 1063–1067, doi:10.1126/science.1155429.

Sullivan, R., et al. (2008), Wind-driven particle mobility on Mars: Insights from Mars Exploration Rover observations at "El Dorado" and surroundings at Gusev crater, *J. Geophys. Res.*, *113*, E06S07, doi:10.1029/2008JE003101.

Waller, D. A., R. Greeley, L. D. Neakrase, G. A. Landis, P. Whelly, and S. D. Thompson (2009), Dust loading in Gusev crater, Mars: Results from two active dust devil seasons, *Eos Trans. AGU*, *90*(52), Fall Meet. Suppl., Abstract EP21A–0579.

Wang, A., et al. (2008), Light-toned salty soils and co-existing silica-rich species discovered by the Mars Exploration Rover Spirit in Columbia Hills, *J. Geophys. Res.*, *113*, E12S40, doi:10.1029/2008JE003126.

Yen, A. S., et al. (2008), Hydrothermal processes at Gusev crater: An evaluation of Paso Robles class soils, *J. Geophys. Res.*, *113*, E06S10, doi:10.1029/2007JE002978.

R. B. Anderson, J. F. Bell III, M. S. Rice, R. Sullivan, and J. J. Wray, Department of Astronomy, Cornell University, Ithaca, NY 14853, USA. (mrice@astro.cornell.edu)

E. A. Cloutis, Department of Geography, University of Winnipeg, 515 Portage Ave., Winnipeg, MB R3B 2E9, Canada.

K. E. Herkenhoff and J. R. Johnson, Astrogeology Science Center, U.S. Geological Survey, Flagstaff, AZ 86001, USA.